



HAL
open science

Microdosimetric calculations of the direct DNA damage induced by low energy electrons using the Geant4-DNA Monte Carlo code

Stefanos Margis, Maria Magouni, Ioanna Kyriakou, Alexandros G. Georgakilas, Sebastien Incerti, Dimitris Emfietzoglou

► To cite this version:

Stefanos Margis, Maria Magouni, Ioanna Kyriakou, Alexandros G. Georgakilas, Sebastien Incerti, et al.. Microdosimetric calculations of the direct DNA damage induced by low energy electrons using the Geant4-DNA Monte Carlo code. *Phys.Med.Biol.*, 2020, 65 (4), pp.045007. 10.1088/1361-6560/ab6b47. hal-02483967

HAL Id: hal-02483967

<https://hal.science/hal-02483967>

Submitted on 8 May 2020

HAL is a multi-disciplinary open access archive for the deposit and dissemination of scientific research documents, whether they are published or not. The documents may come from teaching and research institutions in France or abroad, or from public or private research centers.

L'archive ouverte pluridisciplinaire **HAL**, est destinée au dépôt et à la diffusion de documents scientifiques de niveau recherche, publiés ou non, émanant des établissements d'enseignement et de recherche français ou étrangers, des laboratoires publics ou privés.

Microdosimetric calculations of the direct DNA damage induced by low energy electrons using the Geant4-DNA Monte Carlo code

Stefanos Margis ^a, Maria Magouni ^a, Ioanna Kyriakou ^a, Alexandros G. Georgakilas ^b, Sebastien Incerti ^{c,d} and Dimitris Emfietzoglou ^{a*}

^a *Medical Physics Laboratory, University of Ioannina Medical School, 45110 Ioannina, Greece.*

^b *DNA Damage Laboratory, Physics Department, School of Applied Mathematical and Physical Sciences, National Technical University of Athens (NTUA), Zografou, Athens, Greece.*

^c *University of Bordeaux, CENBG, UMR 5797, F-33170 Gradignan, France.*

^d *CNRS, IN2P3, CENBG, UMR 5797, F-33170 Gradignan, France*

Keywords: Geant4-DNA, microdosimetry, liquid water, DNA damage

*Corresponding author: demfietz@uoi.gr, demfietz@gmail.com

ABSTRACT

Purpose: To calculate the yield of direct DNA damage induced by low energy electrons using Monte Carlo generated microdosimetric spectra at the nanometer scale and examine the influence of various simulation inputs. The potential of classical microdosimetry to offer a viable and simpler alternative to more elaborate mechanistic approaches for practical applications is discussed.

Method: Track-structure simulations with the Geant4-DNA low-energy extension of the Geant4 Monte Carlo toolkit were used for calculating lineal energy spectra in spherical volumes with dimensions relevant to double-strand-break (DSB) induction. The microdosimetric spectra were then used to calculate the yield of simple and clustered DSB based on literature values of the threshold energy of DNA damage. The influence of the different implementations of the dielectric function of liquid water available in Geant4-DNA (Option 2 and Option 4 constructors), as well as the effect of particle tracking cutoff energy and target size are examined.

Results: Frequency- and dose-mean lineal energies in liquid-water spheres of 2, 2.3, 2.6, and 3.4 nm diameter, as well as, number of simple and clustered DSB/Gy/cell are presented for electrons over the 100 eV to 100 keV energy range. Results are presented for both the “default” (Option 2) and “Ioannina” (Option 4) physics models of Geant4-DNA applying several commonly used tracking cutoff energies (10, 20, 50, 100 eV). Overall, the choice of the physics model and target diameter has a moderate effect (up to ~10-30%) on the DSB yield whereas the effect of the tracking cutoff energy may be significant (>100%). Importantly, the yield of both simple and clustered DSB was found to vary significantly (by a factor of 2 or more) with electron energy over the examined range.

Conclusions: The yields of electron-induced simple and clustered DSB exhibit a strong energy dependence over the 100 eV – 100 keV range with implications to radiation quality issues. It is shown that a classical microdosimetry approach for the calculation of DNA damage based on lineal energy spectra in nanometer-size targets predicts comparable results to computationally intensive mechanistic approaches which use detailed atomistic DNA geometries, thus, offering a relatively simple and robust alternative for some practical applications.

1 **1. Introduction**

2 Microdosimetry is useful for investigating radiation quality issues when the relative
3 biological effectiveness (RBE) cannot be deduced directly (ICRU 1983, ICRU 1986). It is
4 widely accepted that the nuclear DNA is one of the most important cellular targets for the
5 biological effects of ionizing radiation (Goodhead 1989, Georgakilas *et al* 2013, Nikjoo *et al*
6 2016b, Schuemann *et al* 2019a). However, experimental measurements of the yield of the
7 various forms of radiation-induced DNA damage, especially of the clustered form, are
8 challenging (Falk *et al* 2010, Nikitaki *et al* 2016). The Monte Carlo (MC) technique, which
9 enables stochastic simulation of radiation tracks in matter, offers an important theoretical tool for
10 quantifying DNA damage induced by different radiation qualities (Hill 1999, Semenenko and
11 Stewart 2004, Bernal and Liendo 2009, Alloni *et al* 2012, Pater *et al* 2014, Nikjoo *et al* 2016b,
12 McNamara *et al* 2017, Friedland *et al* 2017, Liu *et al* 2018, Henthorn *et al* 2018, Chatzipapas *et*
13 *al* 2018, Schuemann *et al* 2019b). The results of such studies depend, mainly, on the physics
14 models used in the MC simulation and the geometrical model used to represent the DNA target.
15 At a more sophisticated level, additional models are included to simulate the chemical stage of
16 radiation action (indirect effect) and the DNA damage/repair processes (Friedland *et al* 2011,
17 Taleei and Nikjoo 2012, Meylan *et al* 2017, Henthorn *et al* 2018, Ramos-Mendez *et al* 2018,
18 Ingram *et al* 2019).

19 The physics models for MC radiation transport simulations are broadly classified as
20 condensed-history (CH) or track-structure (TS) (Andreo 1991, Nikjoo *et al* 2006). In CH models
21 charged-particle transport is simulated via artificial steps (much longer than the mean free path)
22 using multiple-scattering theories (Nahum 1999, Salvat and Fernández-Varea 2009). Thus, the
23 track of the charged particle is “condensed” to fewer simulation steps and energy-loss is assumed

1 to be “continuous” along those steps. As a result, CH models offer a huge reduction in simulation
2 time at the expense of inferior spatial resolution which, in general, is on the order of 0.1-1 mm
3 (Dingfelder 2012, Lazarakis *et al* 2018). In addition, the use of multiple-scattering theories
4 makes CH models most accurate for high-energy charged particles; typically in the MeV energy
5 range. CH models comprise the main physics input of the so-called general-purpose MC codes,
6 such as MCNP (Goorley *et al* 2016), EGS (Kawrakow 2000), GEANT4 (Agostinelli *et al* 2003,
7 Allison *et al* 2006, 2016), FLUKA (Ferrari *et al* 2005), and PENELOPE (Baró *et al* 1995). On
8 the other hand, TS models enable the simulation of radiation tracks in a “discrete” manner,
9 interaction-by-interaction, based on single-scattering cross sections. In principle, TS models can
10 be extended down to very low energies (eV scale) offering superior spatial resolution which may
11 reach the nanometer scale (Dingfelder 2006, Emfietzoglou *et al* 2017a). Although most present
12 day general-purpose codes (see above) enable simulation of hard collisions (i.e. those with large
13 energy- or momentum-transfer) in a discrete manner, the treatment of the remaining (soft)
14 collisions by CH models, limits their validity to electron transport above \approx 0.1-1 keV.

15 It follows from the above discussion that TS models are much better suited for
16 microdosimetry at the subcellular and DNA level compared to CH models. The main drawback
17 of TS models is that they are computer intensive so they are generally limited to low-medium
18 energy charged particles (e.g., typically to electrons below \sim 100 keV). In addition, TS models
19 are far more uncertain, since in the eV-keV energy range, interaction cross sections become very
20 sensitive to the electronic band structure of the material (Dingfelder *et al* 1998, Champion 2003,
21 Dingfelder 2006, Emfietzoglou *et al* 2012, 2017b, Garcia-Molina *et al* 2017) while the
22 underlying assumption of well-defined electron trajectories may also be questioned (Thomson
23 and Kawrakow 2011, 2018, Liljequist and Nikjoo 2014). Among more than a dozen TS codes

1 (partly reviewed in Nikjoo *et al* 2006), PARTRAC (Friedland *et al* 1998, 2011; Dingfelder *et al*
2 2008) and KURBUC (Liamsuwan *et al* 2012; Nikjoo *et al.* 2016a) are perhaps the most known,
3 and include elaborate models of sub-cellular structures as well as explicit DNA damage and
4 repair pathways (Friedland *et al* 2011, Taleei and Nikjoo 2012). Results of TS simulations have
5 been imported in a parameterized form to the Monte Carlo Damage Simulation (MCDS)
6 software (Semenenko and Stewart 2004, 2006) to carry out fast DNA damage calculations for
7 various applications (El Naqa *et al* 2012, Streitmatter *et al* 2017, Stewart *et al* 2015, 2018).

8 Since 2007 Geant4 version 9.1 offers a set of TS models for liquid water through the
9 Geant4-DNA low-energy extension (Incerti *et al* 2010, 2018, Bernal *et al* 2015). The Geant4-
10 DNA package is also the transport engine behind the TOPAS-nBio MC code (Schuemann *et al*
11 2019a). Contrary to the Livermore and Penelope low-energy CH models of Geant4, which are
12 based on atomic (and gas-phase) cross sections and have a recommended electron transport
13 threshold of 250 eV and 100 eV, respectively, the TS models included in the Geant4-DNA
14 package offer ionization and excitation cross sections specific to the liquid phase of water and
15 allow full slowing-down simulations of electron tracks down to ~ 10 eV (Bernal *et al* 2015,
16 Incerti *et al* 2018). The performance of the CH and TS models of Geant4 for micro- and nano-
17 dosimetry has been recently investigated in several studies which reveal important differences at
18 the nano-scale (Incerti *et al* 2016, Kyriakou *et al* 2017, Famulari *et al* 2017, Lazarakis *et al*
19 2018, Kyriakou *et al* 2019, Incerti *et al* 2019).

20 Geometrical models of DNA used in MC simulations vary significantly in terms of
21 complexity. In general, we can distinguish between *amorphous* (structureless) DNA models that
22 use nanometer-size spherical or cylindrical volumes to represent critical dimensions of the DNA
23 target as a whole, and *atomistic* DNA models which account for the three-dimensional geometry

1 and explicit molecular structure of the DNA (e.g., the sugar-phosphate backbone and the
2 individual DNA base-pairs) (Nikjoo and Girard 2012, Friedland *et al* 2008, McNamara *et al*
3 2018).

4 The “amorphous” DNA models are commonly used in the context of *classical* or
5 *regional* microdosimetry (ICRU 1983, Rossi and Zaider 1996). In this approach, stochastic
6 quantities like the specific or lineal energy are calculated by MC simulation in nano- or micro-
7 meter size spherical (or cylindrical) targets and then correlated to DNA damage empirically via
8 consideration of the threshold energy of damage induction (Nikjoo *et al* 2002, 2011). A
9 biophysical foundation for the microdosimetric approach is offered by the Theory of Dual
10 Radiation Action (TDRA) (Kellerer and Rossi 1972, 1978). Specifically, in the “site” version of
11 the TDRA, where the “interaction” probability between pairs of sublesions is independent of
12 their separation distance, the biological effectiveness (i.e., radiation quality) becomes
13 proportional to the integral of the physical (radiation) and geometrical (target) proximity
14 functions. This integral exactly equals the dose-weighted specific (or lineal) energy of the target
15 (Rossi and Zaider 1996). Thus, the “site” version of TDRA offers the biophysical framework for
16 linking microdosimetric spectra to biological damage and, eventually, to radiation quality. Due
17 to its computational simplicity and robustness, classical (or regional) microdosimetry is usually
18 the method of choice for theoretical calculations of the relative biological effectiveness (RBE) of
19 clinical beams/sources (Wuu *et al* 1996, Lindborg and Grindborg 1997, Wu and Zaider 1998,
20 Taschereau *et al* 2003, Lindborg and Nikjoo 2011, Lindborg *et al* 2013, Famulari *et al* 2018). It
21 also forms the basis of the microdosimetric-kinetic-model (MKM) which is used clinically in
22 carbon ion treatment planning systems (Inaniwa *et al* 2010, Bopp *et al* 2016). Microdosimetry

1 has been recognized as providing the physical basis for the definition of the quality factor (Q) in
2 radiation protection (ICRU 1983, ICRU 1986).

3 The atomistic DNA models, on the other hand, are linked to the *mechanistic* approach of
4 DNA damage which attempts to account for the “complete-chain”, i.e., the physical, chemical,
5 and biological stages of radiation action (Nikjoo *et al* 2016b). Despite its sophistication, the
6 mechanistic approach is far less practical because it requires huge computer resources and
7 incorporates a large number of adjustable (and mostly unknown) parameters (Zaider *et al* 1994,
8 Nikjoo *et al* 2016a, Friedland *et al* 2017, Lampe *et al* 2018a, 2018b, Sakata *et al* 2019).

9 It is worth noting that in both the microdosimetric and mechanistic approach a
10 homogeneous liquid water medium is commonly used as a surrogate to the biological medium
11 since it is the dominant constituent of cells (≈ 70% by weight).

12 In the present work, we compare two physics models of Geant4-DNA, namely, the so-
13 called “default” model or Option 2 constructor and the “Ioannina” model or Option 4
14 constructor, which employ different implementations of the dielectric function of liquid water for
15 calculating ionization and excitation cross sections. It should be noted that the current high-
16 energy limits in the two constructors are different, with Opt2 extending up to 1 MeV and Opt4
17 limited up to 10 keV. Lineal energy spectra of low energy electrons (100 eV – 100 keV) in
18 DNA-size volumes are calculated. The microdosimetric spectra are then used to estimate the
19 yield of simple and clustered DNA damage (per Gy and per cell). Low energy electrons are
20 encountered in various therapeutic (e.g., Auger-emitters, low-energy brachytherapy sources) and
21 imaging (e.g., mammography soft X-rays) modalities and have been implicated to the observed
22 increase of RBE for low-energy photon beams/sources (Nikjoo and Lindborg 2010, Stewart *et al*
23 2015, Streitmatter *et al* 2017). Specific aims of the work include: (i) to examine whether the

1 more recent implementation of the dielectric function of liquid water in Geant4-DNA (Ioannina
2 models) influences the simulation of microdosimetric spectra and subsequent DNA damage
3 calculations, (ii) to quantify the degree of which the microdosimetry based calculations of simple
4 and clustered DSB are influenced by some user-defined parameters, such as, the size of the
5 assumed target and the particle tracking cutoff energy, and (iii) to test whether the “classical”
6 microdosimetry approach for calculating DNA damage induction offers a practical alternative to
7 more elaborate mechanistic approaches based on atomistic DNA models.

8

9 **2. Materials and Methods**

10 *2.1. Physics models*

11 In any Geant4 application the user must specify a set of particle processes and physics
12 models that are needed for the particular simulation (i.e., the so-called Physics List). A particle
13 process corresponds to a particular type of physical interaction (e.g., ionization) and can be
14 described by any of several available physics models. These models provide all the needed
15 interaction cross sections (e.g., total, differential in scattering angle and/or energy transfer). To
16 facilitate their use, Geant4 offers interface C++ classes, called “physics constructors”, which
17 contain a list of processes and models for a variety of applications. Regarding the TS simulation
18 of electrons in liquid water, Geant4 offers three sets of physics models, namely, the default
19 Geant4-DNA models (Incerti *et al* 2010) released in Geant4 version 9.1, the models developed at
20 the University of Ioannina (hereafter the “Ioannina” models) (Kyriakou *et al* 2015, 2016) which
21 were released in Geant4 version 10.2, and the so-called CPA100 physics models released in
22 Geant4 version 10.4 (Bordage *et al* 2016). These models are assembled into the
23 G4EmDNAPhysics_option2 (or Opt2), G4EmDNAPhysics_option4 (or Opt4), and

1 G4EmDNAPhysics_option6 (or Opt6) physics constructors, respectively. A fundamental
2 difference between the above constructors concerns the energy-loss models. Specifically, Opt2
3 and Opt4 use the dielectric function of liquid water in order to include condensed-phase effects
4 in the excitation and ionization cross sections whereas Opt6 uses a hybrid model with ionization
5 cross sections pertaining to the gas phase. The details of the different implementation of the
6 dielectric function in Opt2 and Opt4 and their impact upon electron transport have been
7 discussed in some detail elsewhere (Kyriakou *et al* 2015, 2016). Importantly, recent studies have
8 shown that the effect of the different dielectric function implementations on DNA damage
9 induction (Lampe *et al* 2018) and ionization clustering (Villagrasa *et al* 2019) may be
10 significant. The two physics constructor (Opt2 and Opt4) used in the present study are
11 summarized in Table 1. Briefly, ionization and excitation cross sections in Opt2 (default models)
12 and Opt4 (Ioannina models) are calculated from first-principles based on the plane wave Born
13 approximation (PWBA). The target response is considered by a semi-empirical model of the
14 dielectric function of liquid water, $\varepsilon(E, q)$, with E and q being the energy- and momentum-
15 transfer, respectively. The model dielectric function enables to calculate the energy-loss-function
16 (ELF), defined as the imaginary part of the inverse dielectric function, $ELF = Im\left(\frac{-1}{\varepsilon(E, q)}\right)$, which
17 is the main input in the calculation of inelastic cross sections in the PWBA (see Appendix).
18 Since condensed-phase effects are in-built in the dielectric function, inelastic cross section
19 calculations by the ELF are widely considered as the preferred approach for extending high-
20 energy approximations (e.g., Bethe theory) to the sub-keV energies where such effects are
21 pronounced (Emfietzoglou and Nikjoo 2005, 2007). Note that the ELF is not only different for
22 each material but also for the same material in different phases (e.g., gaseous versus liquid
23 water).

1 The principal difference between Opt2 (default models) and Opt 4 (Ioannina models) is
2 on the partitioning of the ELF to the different ionization shells and excitation levels of liquid
3 water (see Appendix). Thus, although the ELF in both Opt2 and Opt4 is based upon the same
4 experimental optical data ($q=0$) and dispersion relations ($q>0$), the two constructors yield
5 noticeable different excitation and ionization cross sections at sub-keV electron energies. The
6 two constructors differ also on the elastic scattering model. Opt2 uses data from partial wave
7 calculations whereas Opt4 relies on the screened Rutherford model with empirical parameters
8 deduced specifically for water (Kyriakou *et al* 2016). Note that the dissociative attachment and
9 vibrational excitation channels available in Opt2 were deactivated for a fair comparison between
10 the two constructors (Opt2 and Opt4). Also, these processes are mostly effective below 10 eV
11 which was the lowest tracking cutoff energy used in the present study.

12
13 **Table 1.** The Geant4-DNA constructors examined in the present work with the corresponding
14 physics models specifically developed for electron TS simulations in liquid water medium.

Constructor	G4EmDNAPhysics_option2	
	(Default models)	
	Model class	Physics model
Ionization	G4DNABornIonizationModel	Emfietzoglou dielectric model (11 eV – 1 MeV)
Excitation	G4DNABornExcitationModel	Emfietzoglou dielectric model (9 eV – 1 MeV)
Elastic scattering	G4DNACHampionElasticModel	Partial Wave Analysis (7.4 eV – 1 MeV)

Constructor	G4EmDNAPhysics_option4	
	(Ioannina models)	
	Model class	Physics model

Ionization	G4DNAEmfietzoglouIonizationModel	Emfietzoglou-Kyriakou dielectric model (10 eV – 10 keV)
Excitation	G4DNAEmfietzoglouExcitationModel	Emfietzoglou-Kyriakou dielectric model (8 eV – 10 keV)
Elastic scattering	G4DNAUeharaScreenedRutherfordElasticModel	Screened Rutherford model (9 eV – 10 keV)

1

2 2.2. Tools and methods

3 Microdosimetry simulations are based on the “microyz” extended example of Geant4-
4 DNA which has been described in detail elsewhere (Kyriakou *et al* 2017, Incerti *et al* 2018).
5 Briefly, for each electron energy presented, 10^6 full slowing-down electron tracks are simulated
6 in an infinite box of liquid water starting from its center. Liquid water is commonly selected as a
7 surrogate of soft tissue since ~70% of the mammalian cells are composed of water (Cooper
8 2000). The primary particles were low energy electrons with initial kinetic energy of 100 eV,
9 200 eV, 300 eV, 500 eV, 700 eV, 1 keV, 2 keV, 5 keV, 10 keV, 20 keV, 50 keV, and 100 keV.

10 Simulations were carried out using tracking cutoff energies of 10 eV, 20 eV, 50 eV, and
11 100 eV. The tracking cut is a particularly important parameter in TS models due to the
12 abundance of very low energy electrons as track-ends (<100 eV). The latter have a very small
13 irradiation range (~few nm) and, therefore, increase the “local” energy deposition along the
14 primary particle track. However, simulating these very low energy electrons is particularly time
15 consuming because of the dominance of the elastic-scattering cross section below ~100 eV. The
16 10 eV value is a common cutoff energy in TS models of liquid water because, to a good
17 approximation, corresponds to the ionization threshold of water in the liquid phase. It is also the
18 low limit of application of Opt4 (see Table 1). Tracking cutoff energies up to 100 eV were also

1 examined because they correspond to the lowest limit of application of some widely-used
2 ionization models of Geant4 (i.e., the Livermore and Penelope sets of models).

3 The targets examined were spheres (which facilitate achieving a uniform and isotropic
4 irradiation) with diameter of 2.0 nm, 2.3 nm, 2.6 nm, and 3.4 nm. This particular range of
5 diameters was chosen as representative of literature values for targets that correspond to (only)
6 direct DNA damage. Specifically, the choice of the smallest diameter (2.0 nm) coincides with the
7 diameter of the B-DNA helix. The 2.3 nm diameter accounts for the additional ~0.3 nm water
8 shell around the DNA helix. The 2.6 nm diameter is a volume-equivalent to a 2.3 nm x 2.3 nm
9 cylinder which is considered a more realistic target geometry for DNA damage studies. Finally,
10 the choice of the largest diameter (3.4 nm) corresponds to the longest distance that a DSB is
11 commonly specified in a straight DNA segment; i.e., 10 base pairs (bp) with bp separation equal
12 to 0.34 nm in B-DNA. Within the present methodology, one may extend the size of the target
13 volume by the diffusion range of an OH radical (e.g., typically ~5-6 nm in the cellular medium)
14 in order to account for the additional DNA damage induced by the indirect effect (radical attack).

15 Simulations have been carried out with Geant4 version 10.2 (patch 01). The statistical
16 uncertainty for the microdosimetric quantities (frequency- and dose-mean lineal energy) was
17 below 0.1% whereas for the DNA damage yield was below 1%. These estimates were deduced
18 from five repeated simulations (of 10^6 histories each) at selected energies and sphere diameters.
19 Additional simulations have also been performed with Geant4 version 10.4 and the most recent
20 10.5 version. In all cases, the discrepancy among the different Geant4 versions was within the
21 statistical uncertainty of the simulations (<1%). This was expected since no changes in the
22 particular constructors (Opt2 and Opt4) has been documented between versions 10.2 and 10.5.

23

1 2.3. DNA damage methodology

2 In the context of classical microdosimetry the calculation of DNA damage yield follows
3 from the stochastic energy deposition in the target volume according to the expression (Nikjoo *et*
4 *al* 1991):

$$5 Y_i = f(\geq E_i) \times \left(\frac{N}{D}\right), \quad [1]$$

6 where E_i is the minimum energy required to induce the i th type of damage (hereafter called
7 threshold energy), $f(\geq E_i)$, is the cumulative probability distribution for energy deposited larger
8 than E_i in the target, N is the number of targets per genome, D is the absorbed dose in the target,
9 and Y_i is the yield of the i th type of damage per unit dose and per cell. Assuming a normal
10 diploid cell with 6.4 Gbp/cell and 0.34 nm/bp, then an approximate value of N may be obtained

11 from the relation $N(\text{cell}^{-1}) = \left(\frac{V_{DNA}}{V_{target}}\right) = \left(\frac{\pi \times (1 \text{ nm})^2 \times 6.4 \times 0.34 (\text{nm})}{\frac{4}{3} \times \pi \times (r (\text{nm}))^3}\right) 10^9$. The absorbed dose in

12 the spherical target equals the frequency-mean specific energy, z_F . For spherical targets a
13 convenient relation is:

$$14 D(\text{Gy}) = z_F(\text{Gy}) = 0.204 \times \frac{y_F(\text{keV}/\mu\text{m})}{d(\mu\text{m})^2}, \quad [2]$$

15 where d is the sphere diameter and y_F is the frequency-mean lineal energy

$$16 y_F = \int_0^\infty y f(y) dy. \quad [3]$$

17 The lineal energy is defined by $y = \varepsilon/\tilde{l}$ where ε is the energy deposited in the target and \tilde{l} is the
18 mean chord length (for spherical volumes $\tilde{l} = \frac{2}{3}d$). Finally, the dose-mean lineal energy y_D ,

19 which is commonly used as a measure of the biological effectiveness, is calculated from

$$20 y_D = \int_0^\infty y d(y) dy = \frac{1}{y_F} \int_0^\infty y^2 f(y) dy. \quad [4]$$

1 The selection of the correct value of the threshold energy is not straightforward due to the
2 lack of available (and conclusive) experimental data. For example, for the induction of single-
3 strand-break (SSB) it is often assumed (based on experimental data) that $E_{SSB} = 17.5$ eV (Nikjoo
4 *et al* 2016a) or $E_{SSB} = 10.79$ eV (Pater *et al* 2014) or that E_{SSB} is a linear function between 5 eV
5 and 37.5 eV (Friedland *et al* 2011). For the induction of double-strand-break (DSB) the situation
6 is even less clear. For example, theoretical studies have indicated that an energy of the order of
7 ~ 100 eV within a ~ 2 -3 nm sphere diameter may be sufficient for inducing a (simple) DSB
8 (Goodhead 1989, Goodhead *et al* 1994, Hill 1999). On the other hand, experiments have
9 indicated that electrons (or photons) with energy as low as ~ 10 eV can still induce DSB, possibly
10 through a resonance mechanism (Prise *et al* 2000, Huels *et al* 2003). In the present work, the
11 DSB threshold energy (E_{DSB}) was deduced by a calibration procedure as follows. There is a
12 general consensus that for low-LET radiation the total yield (direct + indirect) of DSB ranges
13 between 30-60 DSB Gy⁻¹ cell⁻¹ (Semenenko and Stewart 2006, Wang and Rogers 2010, Nikitaki
14 *et al* 2016, Nikjoo *et al* 2016a) with the ratio between direct and indirect effect being
15 approximately 35:65 (Ward 1988). Estimates of the DSB yield from the MCDS version 3.10A
16 (Stewart *et al* 2011, 2015, Stewart 2018) for 100 keV electrons (~ 0.4 keV/ μ m) give a total yield
17 of 52.3 DSB Gy⁻¹ cell⁻¹ (with parameters O₂=21% and DMSO = 0%). Then, an approximate
18 value for the direct contribution can be obtained from MCDS by setting O₂=21% and
19 DMSO=100%, which yields 17.4 DSB Gy⁻¹ cell⁻¹. Note that MCDS predicts a direct-to-indirect
20 ratio equal to 33:67, which is in good agreement with the expected ratio of 35:65 (see above).
21 Thus, to a first approximation, the threshold energy for the induction of (direct) DSB in the
22 present study was deduced by “calibration” to the MCDS data, i.e. matching our calculated DSB
23 yield at 100 keV to the corresponding MCDS yield (17.4 DSB Gy⁻¹ cell⁻¹). This calibration

1 procedure resulted in the following threshold energies for DSB (E_{DSB}) induction for each sphere
 2 size (see Table 2). Interestingly, the E_{DSB} values of Table 2 are fairly in line with the above-
 3 mentioned literature values. It should be mentioned that since the MCDS code provides data also
 4 for the indirect effect, the calibration can be extended to determine the threshold energy for the
 5 induction of DSB from the combined direct plus indirect effect, following also the proper
 6 adjustment (increase) of the target volume by several nanometers due to OH diffusion.

7 More recently, the development of ion-counting detectors that can simulate ionization
 8 cluster-size distributions in nanometer-sized gas volumes has offered an alternative approach to
 9 determine DNA strand break yields (Grosswendt 2004). In this approach, which is often termed
 10 nanodosimetry, the simulated energy deposition by the radiation track (which, in classical
 11 microdosimetry, is used to deduce the damage yield through Eq. [1]) is replaced by the measured
 12 number of ionizations. The latter is empirically correlated, through a statistical model, to the
 13 lesion probability (Garty *et al* 2006).

14

15 **Table 2.** Threshold energies for the induction of direct DSB for each sphere size following
 16 calibration of Eq. (1) to the MCDS value of $Y_i = 17.4 \text{ DSB Gy}^{-1} \text{ cell}^{-1}$ at 100 keV electron
 17 energy.

Diameter of target sphere (nm)	E_{DSB} (eV)
2.0	76
2.3	82
2.6	88
3.4	103.5

18

1 2.4. Clustered DNA damage methodology

2 An important aspect of DNA damage in relation to radiation quality is the degree of its
3 complexity (Ward 1988). It is well-recognized that the more complex the DNA lesions the less
4 likely it is to be repaired faithfully (Georgakilas *et al* 2013). To a first approximation, clustered
5 DNA damage can be considered in the present microdosimetric approach by simply raising the
6 threshold energy according to damage complexity. In this work, we have studied two types of
7 clustered DNA damage (hereafter DSB_c) which are denoted in the literature as DSB^+ and DSB^{++}
8 (Nikjoo *et al* 1997, 1999, 2001). The DSB^+ represents the combination of one DSB and (at least)
9 one SSB within 10 bp, whereas the DSB^{++} represents the combination of (at least) two DSB
10 within 10 bp. Thus, in the present context, the scored volume for DSB_c was assumed to be a
11 sphere of 3.4 nm diameter (in order to encompass 10 bp). The threshold energy of DSB^+ is
12 $E_{DSB^+} = E_{DSB} + E_{SSB^*}$ with $E_{DSB} = 103.5$ eV (see Table 2) and $E_{SSB^*} = 17.5$ eV $\times (3.4/2.3)^3 = 56.5$
13 eV or $E_{SSB^*} = 10.79$ eV $\times (3.4/2.3)^3 = 34.8$ eV. The E_{SSB^*} values are obtained by scaling the SSB
14 threshold energy (17.5 eV or 10.7 eV) associated with a sphere of 2.3 nm diameter (DNA
15 diameter + water shell) to the target sphere of 3.4 diameter which we have here associated to the
16 clustered DNA damage (extending up to 10 bp). On the other hand, the threshold energy of
17 DSB^{++} is simply $E_{DSB^{++}} = 2 \times E_{DSB} = 207$ with $E_{DSB} = 103.5$ eV (see Table 2).

18

19 3. Results and Discussion

20 3.1. Lineal energy

21 In Fig. 1, we present the frequency-mean lineal energy y_F (panel a) and the dose-mean
22 lineal-energy y_D (panel b) as a function of the electron kinetic energy over the 100 eV to 100
23 keV energy range for the different sphere diameters examined. The y_F ranges between ~10-18

1 (keV/ μm) and the y_D between $\sim 17\text{-}27$ (keV/ μm) with the maximum located at ~ 300 eV for all
2 spheres, in good overall agreement with the recent results of Kyriakou *et al* (2017) and Famulari
3 *et al* (2017). Specifically, differences with Kyriakou *et al* (2017) are up to 5% for Opt2 and up to
4 4% for Opt4 and can be attributed to the different cutoff energies while the differences with
5 Famulari *et al* (2017) are up to $\sim 20\%$ and are possibly due to the different physics lists.

6 **FIGURE 1**

7 The dependence of y_F and y_D on the size of the spherical target, with the 2 nm diameter used as
8 baseline, is presented in Fig. 2. Evidently, both quantities are quite sensitive to the size of the
9 sphere and decrease with increasing diameter. For the sphere diameters examined in the present
10 work, the maximum variation is $\sim 30\%$ for y_F and $\sim 20\%$ for y_D .

11 **FIGURE 2**

12 The influence of the physics models on y_F and y_D , with Opt2 constructor (default models) used
13 as baseline, is shown in Fig. 3. Since the upper energy limit of application of Opt4 is 10 keV (see
14 Table 1), the results in Fig. 3 are restricted to the 100 eV – 10 keV energy range. The more
15 recent Opt4 constructor (Ioannina models) is shown to increase both y_F and y_D at all electron
16 energies and for all sphere sizes. The difference between the physics models increases with
17 sphere diameter and it is generally more pronounced at low than at high energies. The observed
18 increase of lineal energy for Opt4 can be attributed to the different implementation of the
19 dielectric function (see Appendix). This leads to a different partitioning of the ELF of Opt2 and
20 Opt4 to the ionization and excitation channels of liquid water which influences primarily the
21 secondary electrons with very low energy (below $\sim 50\text{-}100$ eV), i.e., the track-ends, leading to a
22 more localized energy deposition (Kyriakou *et al* 2015, 2016). However, overall, the effect of
23 physics model on lineal energy remains rather small, i.e., less than 10% for y_F and 8% for y_D .

1 **FIGURE 3**

2 *3.2. DSB yield*

3 The yield of (direct) DSB as a function of the electron kinetic energy over the 100 eV to
4 100 keV energy range and for the different sphere sizes is presented in Fig. 4. For all spheres the
5 DSB yield approaches asymptotically at high electron energies (here 100 keV) the calibration
6 value used in the present work, i.e., 17.4 DSB Gy⁻¹ cell⁻¹ (as per MCDS). As already mentioned,
7 the role of the calibration was to determine the threshold energy of DSB (see Table 2) through
8 Eq. (1). The trend of the DSB yield curve is similar for all spheres and shows a maximum value
9 around 300 eV. The results of Fig. 4 reveal that the variation of the DSB yield over the low
10 electron energy range examined (0.1-100 keV) is significant. Specifically, for the sphere sizes
11 investigated, the yield starts at ~5 DSB Gy⁻¹ cell⁻¹ at 100 eV, then increases rapidly to its
12 maximum of ~40 DSB Gy⁻¹ cell⁻¹ at 300 eV, and then falls gradually to the calibration value of
13 17.4 DSB Gy⁻¹ cell⁻¹ at 100 keV. That is, there is variation of a factor of 2 (or more) of the
14 electron-induced DSB yield over the low energy range. The average initial electron energy from
15 common X-ray imaging modalities and low-energy brachytherapy sources lies roughly between
16 10-100 keV. The results of Fig. 4 indicate that even in this limited energy range between 10-100
17 keV there is a 10-12% variation of the DSB yield.

18 **FIGURE 4**

19 The dependence of the DSB yield on the size of the spherical target, with the 2 nm
20 diameter used as baseline, is presented in Fig. 5. For most of the energy range the effect of target
21 size appears to be modest (up to ~20%), except for the lowest energy (100 eV) where the
22 difference increases rapidly (~50% for d=2.6 nm and ~100% for 3.4 nm). The large differences
23 for 100 eV electrons are because such very low energy electrons are only marginally capable of

1 depositing energy higher than the assumed threshold energy for DSB (E_{DSB} is between 76 eV and
2 103.5 eV for the present sphere sizes; see Table 2). In particular, within the present
3 methodology, in the case of the 3.4 nm sphere, electrons with energy below (or equal to) 100 eV
4 are not capable of inducing DSB since their energy is already below the threshold of 103.5 eV
5 (see Table 2). Obviously, this is a shortcoming of the threshold-energy concept, which is
6 primarily an operational concept, since even very low energy electrons (well below the E_{DSB})
7 have been found capable of inducing DSB (Huels *et al* 2003). Overall, the sensitivity of the DSB
8 yield on the size of the target is comparable to that observed for the lineal energy (y_{F} and y_{D}).

9 **FIGURE 5**

10 The influence of the physics models on the DSB yield, with Opt2 constructor (default
11 models) used as baseline, is shown in Fig. 6. Since the upper energy limit of application of Opt4
12 is 10 keV, the results in Fig. 6 are restricted to the 100 eV – 10 keV energy range. The Opt4
13 constructor (Ioannina models) is shown to increase the DSB yield for all sphere sizes. The effect
14 is more pronounced at low than at high energies and gradually vanishes at energies above 10
15 keV. Similar to the case of the lineal energy (Fig. 3), the larger DSB yield of Opt4 compared to
16 Opt2 can be attributed to the more localized energy deposition (i.e., shorter tracks) due to the
17 different implementation of the dielectric function. It can be seen from Fig. 6 that the different
18 DSB yield between Opt2 and Opt4 increases somewhat with sphere diameter. Overall, the effect
19 of physics models is moderate (up to ~15%) except for the lowest energy (100 eV) where the
20 differences increase rapidly reaching 17% ($d=2$ nm), 20% ($d=2.3$ nm), and 33% ($d=2.6$ nm). By
21 comparing Fig. 3 with Fig. 6, we can observe that the DSB yield is somewhat more sensitivity to
22 the physics model (Opt2 versus Opt4) than the lineal energy (y_{F} and y_{D}) is.

23 **FIGURE 6**

1 meaningful comparison only the direct DSB yield of Lampe *et al* is presented in Fig. 8.
2 Interestingly, the data of Lampe *et al* reveal a much higher sensitivity of the DSB yield on the
3 physics model. Specifically, whereas our DSB yield of Opt2 is very close to the corresponding
4 yield of Lampe *et al*, this is not the case with the DSB yield of Opt4. Specifically, Lampe *et al*
5 predicts a significant increase (~40%) of the direct DSB yield when switching from Opt2 to Opt4
6 whereas in our study the corresponding increase is much smaller (less than 10-15%). This
7 observation indicates that the differences between Opt2 and Opt4 are becoming even more
8 important in mechanistic studies. This is not surprising since the main difference between the
9 two implementations of the dielectric function (Opt2 versus Opt4) is on the relative contribution
10 of excitations and ionizations. Thus, the yield of chemical species is expected to be more
11 sensitive to the choice between Opt2 and Opt4 than the energy deposition stage. Our results are
12 also in fair agreement with those of Bernal *et al* (2015) which are based on an atomistic DNA
13 model using the PENELOPE MC code. On the other hand, sizeable differences are observed
14 between our study and those of Nikjoo *et al* (1997, 1999, 2001), Friedland *et al* (1998), Pater *et*
15 *al* (2014), and Nikitaki *et al* (2016) which may be attributed to the use of different MC codes,
16 physics models, and target geometries, so it is difficult to draw further conclusions. Finally,
17 calculations are also presented for the MCDS version 3.10A (Stewart *et al* 2011) which was used
18 for calibration in our study. As an approximation to the direct DSB yield, the parameters
19 O₂=21% and DMSO=0% were chosen as input to the MCDS calculations. The agreement of our
20 data with the MCDS results is good down to ~300 eV with an average (absolute) difference of
21 about 5% (Opt2) and 9% (Opt4). At even lower energies the MCDS results exhibit a monotonic
22 increase, thus, deviating significantly from our study. In contrast to most other studies, the

1 MCDS code does not seem to predict a peak in the energy dependence of the DSB yield (at least
2 down to 100 eV).

3 **FIGURE 8**

4 *3.3. Effect of tracking cut*

5 All previous results have been obtained using a 10 eV tracking cutoff energy in the MC
6 simulations, i.e., electrons with energy below this value are not further propagated and their
7 residual energy is deposited “at the spot”. In Fig. 9 we have examined the effect of tracking cut
8 on lineal energy (y_F and y_D) for a 2 nm sphere diameter and for electron kinetic energies of 1,
9 10, and 100 keV. The lineal energy data for 10 eV tracking cut are being used as the baseline for
10 comparison. As expected, both y_F and y_D increase with the tracking cutoff energy because fewer
11 secondary electrons are given the chance to escape the target volume, thus, increasing the local
12 energy deposition. As it can be seen, the effect of the tracking cutoff energy is significant; for
13 example, even a small raise from 10 eV to 20 eV increases both y_F and y_D by ~40%, while
14 further increase to 50 eV and 100 eV increases y_F by 80-100% and y_D by 100-150%. Note that a
15 default tracking cutoff energy of the order of 100 eV is commonly used for the low-energy EM
16 models of Geant4 (i.e., the Livermore and Penelope models).

17 **FIGURE 9**

18 The effect of tracking cutoff energy on the DSB yield is shown in Fig. 10 for 1, 10, and
19 100 keV electrons. Evidently, the DSB yield is even more sensitivity to the tracking cut than it is
20 the lineal energy (y_F and y_D). For example, even a small raise of the cutoff energy from 10 eV to
21 20 eV increases the DSB yield by more than 100%. Interestingly, a further increase of the cutoff
22 energy to 50 eV and 100 eV (which represent the low-energy application limits of CH models),
23 increases the DSB yield by ~300-400% and ~500-700%, respectively. The above results clearly

1 reveal the important role of track-ends (i.e., very low energy secondaries below ~100 eV) in
2 DNA damage studies and highlight the need to develop accurate physics models to describe their
3 transport in biological media (Nikjoo *et al* 2016a). From an operational point of view, when
4 different cutoff limits are used (i.e., higher than 10 eV), one should adjust (increase) the
5 threshold energies accordingly in order to compensate for the enhanced DSB yields.

6 **FIGURE 10**

7 *3.4. Clustered DNA damage*

8 The yield of clustered DSB damage (DSB_c) from the direct effect as a function of
9 electron energy is presented in Fig. 11. As explained in section 2.4, in the present work we
10 define clustered DNA damage as $DSB_c = DSB^+ + DSB^{++}$ with $DSB^+ = DSB + SSB$ and $DSB^{++} =$
11 $2 \times DSB$ within 10 bp (Nikjoo *et al* 1997). For each physics model (Opt2 or Opt4) two sets of
12 data for DSB_c are presented, corresponding to the two different threshold energies for the SSB
13 ($E_{SSB} = 10.79$ eV or $E_{SSB} = 17.5$ eV). We can see from Fig. 11 that the DSB_c yield follows the
14 same trend as the DSB yield (Fig. 4), that is, starting from high electron energies it gradually
15 increases with decreasing electron energy reaching a peak around 300 eV and then falls rather
16 rapidly. In absolute values, the ratio of clustered-to-simple DSB yield calculated in our study
17 varies in the range of ~18-33% (for $E_{SSB} = 10.79$ eV) and ~4-16% (for $E_{SSB} = 17.5$ eV) (see
18 Table 3). As expected, with increasing the threshold energy of SSB the yield of clustered DSB
19 damage decreases (here by a factor of ~2 or more).

20

21 **Table 3.** The ratio of clustered-to-simple DSB yield per Gy per cell (expressed as percentage) for
22 two different values of the SSB threshold energy over the examined electron energy range (100
23 eV-100 keV).

	$E_{SSB} = 10.79 \text{ eV}$		$E_{SSB} = 17.5 \text{ eV}$	
Physics model	min (%)	max (%)	min (%)	max (%)
Opt2	18.1	31.9	4.0	15.5
Opt4	20.6	32.8	5.3	16.2

1

2

FIGURE 11

3

4

5

6

7

8

9

10

11

12

13

14

15

16

17

18

19

In the same figure, we have also included for comparison the results of Nikjoo *et al* (1999) and Lampe *et al* (2018a), as well as results from the MCDS version 3.10A (Stewart *et al* 2011). Although there is a sizeable difference among studies, due to different physics models and/or MC codes and methodologies, the general trend of the DSB_c yield as a function of electron energy predicted by Nikjoo *et al* and Lampe *et al* is similar to our study. Interestingly, even in the more difficult case of clustered DNA damage, our results are in fair agreement with those of Lampe *et al* which use a more sophisticated mechanistic approach. As noted also in relation to the DSB yield (Fig. 8), the microdosimetric approach adopted in the present study is not as sensitive to the physics model (Opt2 versus Opt4) as the mechanistic approach of Lampe *et al*. The agreement of our clustered DSB yields with MCDS is not as good as in the case of simple DSB. For example, the average (absolute) difference between our DSB_c data and MCDS in the electron energy range from ~300 eV to 100 keV is ~115% for Opt2 and ~89% for Opt4 when selecting $E_{SSB}=10.79 \text{ eV}$ (case A) and ~18% for Opt2 and ~27% for Opt4 when selecting $E_{SSB}=17.5 \text{ eV}$ (case B). At even lower energies the MCDS results exhibit a monotonic increase, thus, deviating even more from our study.

4. Conclusion

1 The biological importance of the accurate calculation and prediction of complex DNA
2 damage is currently of major importance in the field of radiation biology and radiation protection
3 while also useful for clinical setups and the idea of radiation-induced systemic effects
4 (Mavragani *et al* 2017). In this study a microdosimetric approach has been used to calculate the
5 yield of direct DNA damage, in the form of simple and clustered DSB for low energy electrons.
6 Track-structure simulations were performed with different Geant4-DNA physics models for
7 calculating lineal energy spectra in DNA-size target volumes which were then coupled to
8 empirical values for the threshold energy of SSB and DSB. Overall, the yield of DSB is shown to
9 depend moderately on the physics model and target size while being particularly sensitive to the
10 tracking cutoff energy used in the simulation. A strong dependence on electron energy for both
11 the simple and clustered DSB yield was found which supports the notion of a variable RBE over
12 the photon energy range used in X-ray imaging and low-energy brachytherapy. Perhaps most
13 importantly, it is shown that a classical microdosimetry approach to DNA damage predicts
14 comparable results to computationally intensive mechanistic approaches, thus, offering a
15 relatively simple and robust alternative for some practical applications of radiation quality.

16

17 **Acknowledgement**

18 We would like to acknowledge financial support from the France-Greece “Project International
19 de Cooperation Scientifique (PICS)” #8235. I. Kyriakou and D. Emfietzoglou acknowledge
20 financial support from European Space Agency (ESA Contract No. 4000112863/14/NL/HB).

21

1 Appendix

2 The calculation of inelastic cross sections for non-relativistic electrons by the Opt2 and Opt4
 3 constructors of Geant4-DNA is based on the following expression of the first Born
 4 approximation (Nikjoo *et al* 2016a):

$$5 \frac{d^2\sigma_{\text{Born}}}{dEdq} = \frac{1}{\pi a_0 N T} \frac{1}{q} \left\{ \frac{\text{Im}[\varepsilon(E, q)]}{\text{Re}[\varepsilon(E, q)]^2 + \text{Im}[\varepsilon(E, q)]^2} \right\}, \quad [A1]$$

6 where a_0 is the Bohr radius, T is the electron kinetic energy, N is the density of target centers
 7 (here water molecules), E is the energy-transfer, q is the momentum-transfer, $\varepsilon(E, q)$ is the
 8 dielectric function, and $\text{Im}[-1/\varepsilon(E, q)] = \text{Im}[\varepsilon(E, q)] / \{\text{Re}[\varepsilon(E, q)]^2 + \text{Im}[\varepsilon(E, q)]^2\}$ is the ELF.
 9 Integration of Eq. [A1] over q gives the differential energy-loss cross sections, and a subsequent
 10 integration over E gives inverse inelastic mean free paths ($= N\sigma$). In Opt2 the imaginary part of
 11 the dielectric function at the optical limit (equivalent to the photoabsorption spectrum) is
 12 partitioned to the individual ionization shells and excitation levels according to (Kyriakou *et al*
 13 2015, 2016):

$$14 \text{Im}[\varepsilon(E, q = 0)]_{\text{Opt2}} = \sum_n^{\text{ioniz.}} \text{Im}[\varepsilon_n(E, q = 0)] + \sum_k^{\text{excit.}} \text{Im}[\varepsilon_k(E, q = 0)]$$

$$= \sum_n^{\text{ioniz.}} [D_n(E; E_n) \Theta(E - B_n)] + \sum_k^{\text{excit.}} [D_k^*(E; E_k) \Theta(E - B_k)] \quad [A2]$$

15 where $D_n(E; E_n)$ and $D_k^*(E; E_k)$ are ionization and excitation Drude functions, respectively, and
 16 $B_{n,k}$ are threshold energies (e.g., binding energies for ionization shells). However, as discussed
 17 elsewhere (Kyriakou *et al.* 2015, 2016), the implementation of Eq. [A2] results in partial
 18 violation of the f-sum-rule and an incorrect calculation of the real part of the dielectric function,
 19 $\text{Re}[\varepsilon(E, q = 0)]$, through the Kramers-Kronig relation. The above deficiencies are overcome in
 20 Opt4 by replacing Eq. [A2] by the expression (Kyriakou *et al* 2015, 2016):

$$\begin{aligned}
\text{Im}[\varepsilon(E, q = 0)]_{\text{Opt4}} &= \sum_n^{\text{ioniz.}} \text{Im}[\varepsilon_n(E, q = 0)] + \sum_k^{\text{excit.}} \text{Im}[\varepsilon_k(E, q = 0)] \\
&= \sum_n^{\text{ioniz.}} \{ [D_n(E; E_n) - D_n(E; B_n) \exp(B_n - E) + F_n(E)] \Theta(E - B_n) \}, \quad \text{A[3]} \\
&\quad + \sum_k^{\text{excit.}} \{ [D_k^*(E; E_k) + F_k(E)] \Theta(E - B_k) \}
\end{aligned}$$

2 where $D_n(E; B_n) \exp(B_n - E)$ is an exponential smoothing function for ionisations, and $F_{n,k}(E)$
3 are contributions due to the truncation of the ionization Drude functions at the corresponding
4 threshold energies. Despite starting from essentially the same optical data for $\varepsilon(E, q = 0)$, the
5 ELF's resulting from Eq. [A2] (used in Opt2) and Eq. [A3] (used in Opt4) yield substantially
6 different ionisation and excitation cross sections calculated by Eq. [A1]. In particular, since
7 $F_{n,k}(E)$ are positive-value functions, Eq. [A3] leads to an increased contribution of the
8 excitation channels relative to ionizations (Kyriakou *et al* 2015, 2016).

9

1 REFERENCES

- 2 Agostinelli S, Allison J, Amako K, Apostolakis J, Araujo H, Arce P, Asai M, Axen D, Banerjee
3 S, Barrand G, Behner F, Bellagamba L, Boudreau J, Broglia L, Brunengo A, Burkhardt
4 H, Chauvie S, Chuma J, Chytracsek R, Cooperman G, Cosmo G, Degtyarenko P,
5 Dell'Acqua A, Depaola G, Dietrich D, Enami R, Feliciello A, Ferguson C, Fesefeldt H,
6 Folger G, Foppiano F, Forti A, Garelli S, Giani S, Giannitrapani R, Gibin D, Gómez
7 Cadenas J J, González I, Gracia Abril G, Greeniaus G, Greiner W, Grichine V,
8 Grossheim A, Guatelli S, Gumplinger P, Hamatsu R, Hashimoto K, Hasui H, Heikkinen
9 A, Howard A, Ivanchenko V, Johnson A, Jones F W, Kallenbach J, Kanaya N, Kawabata
10 M, Kawabata Y, Kawaguti M, Kelner S, Kent P, Kimura A, Kodama T, Kokoulin R,
11 Kossov M, Kurashige H, Lamanna E, Lampén T, Lara V, Lefebure V, Lei F, Liendl M,
12 Lockman W, Longo F, Magni S, Maire M, Medernach E, Minamimoto K, Mora de
13 Freitas P, Morita Y, Murakami K, Nagamatu M, Nartallo R, Nieminen P, Nishimura T,
14 Ohtsubo K, Okamura M, O'Neale S, Oohata Y, Paech K, Perl J, Pfeiffer A, Pia M G,
15 Ranjard F, Rybin A, Sadilov S, Di Salvo E, Santin G, Sasaki T, et al 2003 Geant4—a
16 simulation toolkit *Nuclear Instruments and Methods in Physics Research Section A:
17 Accelerators, Spectrometers, Detectors and Associated Equipment* **506** 250–303
- 18 Allison J, Amako K, Apostolakis J, Araujo H, Arce Dubois P, Asai M, Barrand G, Capra R,
19 Chauvie S, Chytracsek R, Cirrone G A P, Cooperman G, Cosmo G, Cuttone G, Daquino G
20 G, Donszelmann M, Dressel M, Folger G, Foppiano F, Generowicz J, Grichine V,
21 Guatelli S, Gumplinger P, Heikkinen A, Hrivnacova I, Howard A, Incerti S, Ivanchenko
22 V, Johnson T, Jones F, Koi T, Kokoulin R, Kossov M, Kurashige H, Lara V, Larsson S,
23 Lei F, Link O, Longo F, Maire M, Mantero A, Mascialino B, McLaren I, Mendez
24 Lorenzo P, Minamimoto K, Murakami K, Nieminen P, Pandola L, Parlati S, Peralta L,
25 Perl J, Pfeiffer A, Pia M G, Ribon A, Rodrigues P, Russo G, Sadilov S, Santin G, Sasaki
26 T, Smith D, Starkov N, Tanaka S, Tcherniaev E, Tome B, Trindade A, Truscott P, Urban
27 L, Verderi M, Walkden A, Wellisch J P, Williams D C, Wright D and Yoshida H 2006
28 Geant4 developments and applications *IEEE Transactions on Nuclear Science* **53** 270–8
- 29 Allison J, Amako K, Apostolakis J, Arce P, Asai M, Aso T, Bagli E, Bagulya A, Banerjee S,
30 Barrand G, Beck B R, Bogdanov A G, Brandt D, Brown J M C, Burkhardt H, Canal Ph,
31 Cano-Ott D, Chauvie S, Cho K, Cirrone G A P, Cooperman G, Cortés-Giraldo M A,
32 Cosmo G, Cuttone G, Depaola G, Desorgher L, Dong X, Dotti A, Elvira V D, Folger G,
33 Francis Z, Galoyan A, Garnier L, Gayer M, Genser K L, Grichine V M, Guatelli S,
34 Guèye P, Gumplinger P, Howard A S, Hřivnáčová I, Hwang S, Incerti S, Ivanchenko A,
35 Ivanchenko V N, Jones F W, Jun S Y, Kaitaniemi P, Karakatsanis N, Karamitros M,
36 Kelsey M, Kimura A, Koi T, Kurashige H, Lechner A, Lee S B, Longo F, Maire M,
37 Mancusi D, Mantero A, Mendoza E, Morgan B, Murakami K, Nikitina T, Pandola L,
38 Paprocki P, Perl J, Petrović I, Pia M G, Pokorski W, Quesada J M, Raine M, Reis M A,
39 Ribon A, Ristić Fira A, Romano F, Russo G, Santin G, Sasaki T, Sawkey D, Shin J I,
40 Strakovsky I I, Taborda A, Tanaka S, Tomé B, Toshito T, Tran H N, Truscott P R, Urban
41 L, Uzhinsky V, Verbeke J M, Verderi M, Wendt B L, Wenzel H, Wright D H, Wright D
42 M, Yamashita T, Yarba J, et al 2016 Recent developments in Geant 4 *Nuclear
43 Instruments and Methods in Physics Research Section A: Accelerators, Spectrometers,
44 Detectors and Associated Equipment* **835** 186–225

- 1 Alloni D, Campa A, Friedland W, Mariotti L and Ottolenghi A 2012 Track structure, radiation
2 quality and initial radiobiological events: Considerations based on the PARTRAC code
3 experience *International Journal of Radiation Biology* **88** 77–86
- 4 Andreo P 1991 Monte Carlo techniques in medical radiation physics *Physics in Medicine and
5 Biology* **36** 861–920
- 6 Baró J, Sempau J, Fernández-Varea J M and Salvat F 1995 PENELOPE: An algorithm for
7 Monte Carlo simulation of the penetration and energy loss of electrons and positrons in
8 matter *Nuclear Instruments and Methods in Physics Research Section B: Beam
9 Interactions with Materials and Atoms* **100** 31–46
- 10 Bernal M A, Bordage M C, Brown J M C, Davidková M, Delage E, El Bitar Z, Enger S A,
11 Francis Z, Guatelli S, Ivanchenko V N, Karamitros M, Kyriakou I, Maigne L, Meylan S,
12 Murakami K, Okada S, Payno H, Perrot Y, Petrovic I, Pham Q T, Ristic-Fira A, Sasaki T,
13 Štěpán V, Tran H N, Villagrana C and Incerti S 2015 Track structure modeling in liquid
14 water: A review of the Geant4-DNA very low energy extension of the Geant4 Monte
15 Carlo simulation toolkit *Physica Medica* **31** 861–74
- 16 Bernal M A and Liendo J A 2009 An investigation on the capabilities of the PENELOPE MC
17 code in nanodosimetry: PENELOPE code in nanodosimetry *Medical Physics* **36** 620–5
- 18 Bopp C, Hirayama R, Inaniwa T, Kitagawa A, Matsufuji N and Noda K 2016 Adaptation of the
19 microdosimetric kinetic model to hypoxia *Physics in Medicine and Biology* **61** 7586–99
- 20 Bordage M C, Bordes J, Edel S, Terrissol M, Franceries X, Bardiès M, Lampe N and Incerti S
21 2016 Implementation of new physics models for low energy electrons in liquid water in
22 Geant4-DNA *Physica Medica* **32** 1833–40
- 23 Champion C 2003 Theoretical cross sections for electron collisions in water: structure of electron
24 tracks *Physics in Medicine and Biology* **48** 2147–68
- 25 Chatzipapas K P, Papadimitroulas P, Obeidat M, McConnell K A, Kirby N, Loudos G,
26 Papanikolaou N and Kagadis G C 2018 Quantification of DNA double strand breaks
27 using Geant4-DNA *Medical Physics* **46** 405-13
- 28 Cooper G M 2000 *The cell: a molecular approach* (Washington, DC: ASM Press)
- 29 Dingfelder M 2006 Track structure: time evolution from physics to chemistry *Radiation
30 Protection Dosimetry* **122** 16–21
- 31 Dingfelder M 2012 Track-Structure Simulations for Charged Particles *Health Phys* **103**
- 32 Dingfelder M, Hantke D, Inokuti M and Paretzke H G 1998 Electron inelastic-scattering cross
33 sections in liquid water *Radiation Physics and Chemistry* **53** 1–18
- 34 Dingfelder M, Ritchie R H, Turner J E, Friedland W, Paretzke H G and Hamm R N 2008
35 Comparisons of calculations with PARTRAC and NOREC: transport of electrons in
36 liquid water *Radiat. Res.* **169** 584–94
- 37 El Naqa I, Pater P and Seuntjens J 2012 Monte Carlo role in radiobiological modelling of
38 radiotherapy outcomes *Phys Med Biol* **57** R75-97
- 39 Emfietzoglou D, Nikjoo H 2005 The effect of model approximations on single-collision
40 distributions of low-energy electrons in liquid water *Radiation Research* **163** 98-111
- 41 Emfietzoglou D, Nikjoo H 2007 Accurate electron inelastic cross sections and stopping powers
42 for liquid water over the 0.1-10 keV range based on an improved dielectric description of
43 the Bethe surface *Radiation Research* **167** 110-120
- 44 Emfietzoglou D, Kyriakou I, Abril I, Garcia-Molina R and Nikjoo H 2012 Inelastic scattering of
45 low-energy electrons in liquid water computed from optical-data models of the Bethe
46 surface *International Journal of Radiation Biology* **88** 22–8

- 1 Emfietzoglou D, Kyriakou I, Garcia-Molina R and Abril I 2017a Inelastic mean free path of low-
2 energy electrons in condensed media: beyond the standard models: Low-energy electron
3 inelastic mean free paths *Surface and Interface Analysis* **49** 4–10
- 4 Emfietzoglou D, Papamichael G and Nikjoo H 2017b Monte Carlo Electron Track Structure
5 Calculations in Liquid Water Using a New Model Dielectric Response Function
6 *Radiation Research* **188** 355–68
- 7 Falk M, af Rosenschöld P M, Keall P, Cattell H, Cho B C, Poulsen P, Povzner S, Sawant A,
8 Zimmerman J and Korreman S 2010 Real-time dynamic MLC tracking for inversely
9 optimized arc radiotherapy *Radiotherapy and Oncology* **94** 218–23
- 10 Famulari G, Pater P and Enger S A 2018 Microdosimetric Evaluation of Current and Alternative
11 Brachytherapy Sources—A Geant4-DNA Simulation Study *International Journal of*
12 *Radiation Oncology • Biology • Physics* **100** 270–7
- 13 Famulari G, Pater P and Enger S A 2017 Microdosimetry calculations for monoenergetic
14 electrons using Geant4-DNA combined with a weighted track sampling algorithm
15 *Physics in Medicine & Biology* **62** 5495–508
- 16 Ferrari A, Sala P R, Fasso A and Ranft J 2005 *FLUKA: A Multi-Particle Transport Code* Online:
17 <http://www.osti.gov/servlets/purl/877507-sC9S9L/>
- 18 Frankenberg D, Goodhead D T, Frankenberg-Schwager M, Harbich R, Bance D A, Wilkinson R
19 E 1986 Effectiveness of 1.5 keV aluminium K and 0.3 carbon K characteristic X-rays at
20 inducing DNA double-strand breaks in yeast cells *Int J Radiat Biol* **50** 727–741
- 21 Friedland W, Dingfelder M, Kunderát P and Jacob P 2011 Track structures, DNA targets and
22 radiation effects in the biophysical Monte Carlo simulation code PARTRAC *Mutation*
23 *Research/Fundamental and Molecular Mechanisms of Mutagenesis* **711** 28–40
- 24 Friedland W, Paretzke H G, Ballarini F, Ottolenghi A, Kreth G and Cremer C 2008 First steps
25 towards systems radiation biology studies concerned with DNA and chromosome
26 structure within living cells *Radiation and Environmental Biophysics* **47** 49–61
- 27 Friedland W, Schmitt E, Kunderát P, Dingfelder M, Baiocco G, Barbieri S and Ottolenghi A 2017
28 Comprehensive track-structure based evaluation of DNA damage by light ions from
29 radiotherapy-relevant energies down to stopping *Scientific Reports* **7** 45161
- 30 Friedland W, Jacob P, Paretzke H G, and Stork T 1998 Monte Carlo simulation of the production
31 of short DNA fragments by low-linear energy transfer radiation using high-order DNA
32 molecules *Radiat Res* **150** 170–182
- 33 Garcia-Molina R, Abril I, Kyriakou I and Emfietzoglou D 2017 Inelastic scattering and energy
34 loss of swift electron beams in biologically relevant materials: Energy loss of electron
35 beams in biomaterials *Surface and Interface Analysis* **49** 11–7
- 36 Garty G, Schulte R, Shchemelinin S, Grosswendt B, Leloup C, Assaf G, Breskin A, Chechik R
37 and Bashkirov V 2006 First attempt at prediction of DNA strand-break yields using
38 nanodosimetric data *Radiat Prot Dosim* **122** 451–454
- 39 Georgakilas A G, O’Neill P and Stewart R D 2013 Induction and Repair of Clustered DNA
40 Lesions: What Do We Know So Far? *Radiation Research* **180** 100–9
- 41 Goodhead D T 1989 The Initial Physical Damage Produced by Ionizing Radiations *International*
42 *Journal of Radiation Biology* **56** 623–34
- 43 Goodhead D T, Leenhouts H P, Paretzke H G, Terrissol M, Nikjoo H and Blaauboer R 1994
44 Track Structure Approaches to the Interpretation of Radiation Effects on DNA *Radiation*
45 *Protection Dosimetry* **52** 217–23

- 1 Goorley T, James M, Booth T, Brown F, Bull J, Cox L J, Durkee J, Elson J, Fensin M, Forster R
2 A, Hendricks J, Hughes H G, Johns R, Kiedrowski B, Martz R, Mashnik S, McKinney G,
3 Pelowitz D, Prael R, Sweezy J, Waters L, Wilcox T and Zukaitis T 2016 Features of
4 MCNP6 *Annals of Nuclear Energy* **87** 772–83
- 5 Grosswendt B 2004 Recent advances of nanodosimetry *Radiat Prot Dosim* **110** 845-850
- 6 Henthorn N T, Warmenhoven J W, Sotiropoulos M, Mackay R I, Kirkby N F, Kirkby K J and
7 Merchant M J 2018 In Silico Non-Homologous End Joining Following Ion Induced DNA
8 Double Strand Breaks Predicts That Repair Fidelity Depends on Break Density *Scientific*
9 *Reports* **8** 2654
- 10 Hill M A 1999 Radiation damage to DNA: The importance of track structure *Radiation*
11 *Measurements* **31** 15–23
- 12 Huels M A, Boudaïffa B, Cloutier P, Hunting D and Sanche L 2003 Single, Double, and
13 Multiple Double Strand Breaks Induced in DNA by 3–100 eV Electrons *Journal of the*
14 *American Chemical Society* **125** 4467–77
- 15 ICRU 36 1983 Microdosimetry *Journal of the International Commission on Radiation Units and*
16 *Measurements*, **19** <https://doi.org/10.1093/jicru/os19.1.Report36>
- 17 ICRU 40 1986 The Quality Factor in Radiation Protection *Journal of the International*
18 *Commission on Radiation Units and Measurements*,
19 **21** <https://doi.org/10.1093/jicru/os21.1.Report40>
- 20 Inaniwa T, Furukawa T, Kase Y, Matsufuji N, Toshito T, Matsumoto Y, Furusawa Y and Noda
21 K 2010 Treatment planning for a scanned carbon beam with a modified microdosimetric
22 kinetic model *Physics in Medicine and Biology* **55** 6721–37
- 23 Incerti S, Douglass M, Penfold S, Guatelli S and Bezak E 2016 Review of Geant4-DNA
24 applications for micro and nanoscale simulations *Physica Medica* **32** 1187–200
- 25 Incerti S, Baldacchino G, Bernal M, Capra R, Champion C, Francis Z, Guatelli S, Guèye P,
26 Mantero A, Mascialino B, Moretto P, Nieminen P, Rosenfeld A, Villagrasa C and
27 Zacharatou C 2010 The Geant4-DNA project. *International Journal of Modeling*
28 *Simulation and Scientific Computing* **1** 157–78
- 29 Incerti S, Ivanchenko A, Karamitros M, Mantero A, Moretto P, Tran H N, Mascialino B,
30 Champion C, Ivanchenko V N, Bernal M A, Francis Z, Villagrasa C, Baldacchino G,
31 Guèye P, Capra R, Nieminen P and Zacharatou C 2010 Comparison of GEANT4 very
32 low energy cross section models with experimental data in water *Medical Physics* **37**
33 4692–708
- 34 Incerti S, Kyriakou I, Bernal M A, Bordage M C, Francis Z, Guatelli S, Ivanchenko V,
35 Karamitros M, Lampe N, Lee S B, Meylan S, Min C H, Shin W G, Nieminen P, Sakata
36 D, Tang N, Villagrasa C, Tran H N and Brown J M C 2018 Geant4-DNA example
37 applications for track structure simulations in liquid water: A report from the Geant4-
38 DNA Project *Medical Physics* **45** e722–39
- 39 Incerti S, Kyriakou I, Bordage M C, Guatelli S, Ivanchenko V and Emfietzoglou D 2019 Track
40 structure simulations of proximity functions in liquid water using the Geant4-DNA
41 toolkit *Journal of Applied Physics* **125** 104301
- 42 Ingram S P, Warmenhoven J W, Henthorn N T, Smith E A K, Chadwick A L, Burnet N G,
43 Mackay R I, Kirkby N F, Kirkby K J and Merchant M J 2019 Mechanistic modelling
44 supports entwined rather than exclusively competitive DNA double-strand break repair
45 pathway *Scientific Reports* **9** 6359

- 1 Kawrakow I 2000 Accurate condensed history Monte Carlo simulation of electron transport. I.
2 EGS nrc, the new EGS4 version *Medical Physics* **27** 485–98
- 3 Kellerer A M and Rossi H H 1978 A Generalized Formulation of Dual Radiation Action
4 *Radiation Research* **75** 471
- 5 Kellerer A M and Rossi H H 1972 The theory of dual radiation action *Radiat. Res.* **8** 85
- 6 Kyriakou I, Emfietzoglou D, Ivanchenko V, Bordage M C, Guatelli S, Lazarakis P, Tran H N
7 and Incerti S 2017 Microdosimetry of electrons in liquid water using the low-energy
8 models of Geant4 *Journal of Applied Physics* **122** 024303
- 9 Kyriakou I, Incerti S and Francis Z 2015 Technical Note: Improvements in GEANT 4 energy-loss
10 model and the effect on low-energy electron transport in liquid water: Low-energy
11 electron energy-loss model *Medical Physics* **42** 3870–6
- 12 Kyriakou I, Ivanchenko V, Sakata D, Bordage M C, Guatelli S, Incerti S and Emfietzoglou D
13 2019 Influence of track structure and condensed history physics models of Geant4 to
14 nanoscale electron transport in liquid water *Physica Medica* **58** 149–54
- 15 Kyriakou I, Šefl M, Nourry V and Incerti S 2016 The impact of new Geant4-DNA cross section
16 models on electron track structure simulations in liquid water *Journal of Applied Physics*
17 **119** 194902
- 18 Lampe N, Karamitros M, Breton V, Brown J M C, Kyriakou I, Sakata D, Sarramia D and Incerti
19 S 2018a Mechanistic DNA damage simulations in Geant4-DNA part 1: A parameter
20 study in a simplified geometry *Physica Medica* **48** 135–45
- 21 Lampe N, Karamitros M, Breton V, Brown J M C, Sakata D, Sarramia D and Incerti S 2018b
22 Mechanistic DNA damage simulations in Geant4-DNA Part 2: Electron and proton
23 damage in a bacterial cell *Physica Medica* **48** 146–55
- 24 Lazarakis P, Incerti S, Ivanchenko V, Kyriakou I, Emfietzoglou D, Corde S, Rosenfeld A B,
25 Lerch M, Tehei M and Guatelli S 2018 Investigation of track structure and condensed
26 history physics models for applications in radiation dosimetry on a micro and nano scale
27 in Geant4 *Biomedical Physics & Engineering Express* **4** 024001
- 28 Liamsuwan T, Emfietzoglou D, Uehara S and Nikjoo H 2012 Microdosimetry of low-energy
29 electrons *International Journal of Radiation Biology* **88** 899–907
- 30 Liljequist D and Nikjoo H 2014 On the validity of the trajectory methods for calculating the
31 transport of very low energy (<1 keV) electrons in liquids and amorphous media
32 *Radiation Physics and Chemistry* **99** 45–52
- 33 Lindborg L, Hultqvist M, Carlsson Tedgren Å and Nikjoo H 2013 Lineal energy and radiation
34 quality in radiation therapy: model calculations and comparison with experiment *Physics
35 in Medicine and Biology* **58** 3089–105
- 36 Lindborg L and Nikjoo H 2011 Microdosimetry and radiation quality determinations in radiation
37 protection and radiation therapy *Radiation Protection Dosimetry* **143** 402–8
- 38 Lindborg L and Grindborg J-E 1997 Nanodosimetric results and radiotherapy beams: A clinical
39 application? *Radiation Protection Dosimetry* **1-4** 541–6
- 40 Liu W, Tan Z, Zhang L and Champion C 2018 Investigation on the correlation between energy
41 deposition and clustered DNA damage induced by low-energy electrons *Radiat Environ
42 Biophys* **57** 179–87
- 43 Meylan S, Incerti S, Karamitros M, Tang N, Bueno M, Clairard I, Villagrasa C 2017 Simulation
44 of early DNA damage after the irradiation of a fibroblast cell nucleus using Geant4-DNA
45 *Sci Rep* **7** 11923

- 1 Mavragani I, Nikitaki Z, Souli M, Aziz A, Newsheen S, Aziz K, Rogakou E and Georgakilas A
2 2017 Complex DNA Damage: A Route to Radiation-Induced Genomic Instability and
3 Carcinogenesis *Cancers* **9** 91
- 4 McNamara A, Geng C, Turner R, Ramos-Mendez J, Perl J, Held K, Faddegon B, Paganetti H
5 and Schuemann J 2017 Validation of the radiobiology toolkit TOPAS-nBio in simple
6 DNA geometries *Physica Medica* **33** 207–15
- 7 McNamara A, Ramos-Mendez J, Perl J, Held K, Dominguez N, Moreno E, Henthorn N T,
8 Kirkby K J, Meylan S, Villagrasa C, Incerti S, Faddegon B, Paganetti H and Schuemann
9 J 2018 Geometrical structures for radiation biology research as implemented in TOPAS-
10 nBio toolkit *Physics in Medicine and Biology* **63** 175018
- 11 Nahum A E 1999 Condensed-history Monte-Carlo simulation for charged particles: what can it
12 do for us? *Radiat Environ Biophys* **38** 163–73
- 13 Nikitaki Z, Nikolov V, Mavragani I V, Mladenov E, Mangelis A, Laskaratou D A, Fragkoulis G
14 I, Hellweg C E, Martin O A, Emfietzoglou D, Hatzi V I, Terzoudi G I, Iliakis G and
15 Georgakilas A G 2016 Measurement of complex DNA damage induction and repair in
16 human cellular systems after exposure to ionizing radiations of varying linear energy
17 transfer (LET) *Free Radical Research* **50** S64–78
- 18 Nikjoo H, Emfietzoglou D, Liamsuwan T, Taleei R, Liljequist D and Uehara S 2016a Radiation
19 track, DNA damage and response—a review *Reports on Progress in Physics* **79** 116601
- 20 Nikjoo H, Taleei R, Liamsuwan T, Liljequist D and Emfietzoglou D 2016b Perspectives in
21 radiation biophysics: From radiation track structure simulation to mechanistic models of
22 DNA damage and repair *Radiation Physics and Chemistry* **128** 3–10
- 23 Nikjoo H and Girard P 2012 A model of the cell nucleus for DNA damage calculations
24 *International Journal of Radiation Biology* **88** 87–97
- 25 Nikjoo H, Goorley T, Fulford J, Takakura K and Ito T 2002 Quantitative Analysis of Energetics
26 of DNA Damage *Radiation Protection Dosimetry* **99** 91–8
- 27 Nikjoo H and Lindborg L 2010 RBE of low energy electrons and photons *Physics in Medicine
28 and Biology* **55** R65–109
- 29 Nikjoo H, O’Neill P, Terrissol M and Goodhead D T 1999 Quantitative modelling of DNA
30 damage using Monte Carlo track structure method *Radiation and Environmental
31 Biophysics* **38** 31–8
- 32 Nikjoo H, O’Neill P, Wilson W E and Goodhead D T 2001 Computational Approach for
33 Determining the Spectrum of DNA Damage Induced by Ionizing Radiation *Radiation
34 Research* **156** 577–83
- 35 Nikjoo H, Uehara S, Emfietzoglou D and Cucinotta F A 2006 Track-structure codes in radiation
36 research *Radiation Measurements* **41** 1052–74
- 37 Nikjoo H, Uehara S, Emfietzoglou D and Pinsky L 2011 A database of frequency distributions of
38 energy depositions in small-size targets by electrons and ions *Radiation Protection
39 Dosimetry* **143** 145–51
- 40 Nikjoo H, O’Neill P, Goodhead D T 1997 Computational modelling of low-energy electron-
41 induced DNA damage by early physical and chemical events *International Journal of
42 Radiation Biology* **71** 467–83
- 43 Nikjoo H, Goodhead D T, Charlton D E and Paretzke H G 1991 Energy deposition in small
44 cylindrical targets by monoenergetic electrons *Int J Radiat Biol* **60** 739-756

- 1 Pater P, Seuntjens J, El Naqa I and Bernal M A 2014 On the consistency of Monte Carlo track
2 structure DNA damage simulations: Consistency of MCTS DNA damage simulations
3 *Medical Physics* **41** 121708
- 4 Prise K M, Folkard M, Michael B D, Vojnovic B, Brocklehurst B, Hopkirk A and Munro I H
5 2000 Critical energies for SSB and DSB induction in plasmid DNA by low-energy
6 photons: action spectra for strand-break induction in plasmid DNA irradiated in vacuum
7 *Int. J. Radiat. Biol.* **76** 881–90
- 8 Ramos-Mendez J, Perl J, Schuemann J, McNamara A, Paganetti H, Faddegon B 2018 Monte
9 Carlo simulation of chemistry following radiolysis with TOPAS-nBio *Physics in*
10 *Medicine and Biology* **63** 105014
- 11 Rossi H H and Zaider M 1996 *Microdosimetry and Its Applications* (Berlin, Heidelberg:
12 Springer Berlin Heidelberg) Online: <http://link.springer.com/10.1007/978-3-642-85184-1>
- 13 Sakata D, Lampe N, Karamitros M, Kyriakou I, Belovg O, Bernal M A, Bolst D, Bordage M-C,
14 Breton V, Brown J M C, Francis Z, Ivanchenko V, Meylan S, Murakami K, Okada S,
15 Petrovic I, Ristic-Fira A, Santin G, Sarrami D, Sasaki T, Shin W-G, Tang N, Trant H N,
16 Villagrasa C, Emfietzoglou D, Nieminen P, Guatelli S, Incerti S. 2019 Evaluation of
17 early radiation DNA damage in a fractal cell nucleus model using Geant4-DNA *Physica*
18 *Medica* **62**, 152-7
- 19 Salvat F and Fernández-Varea J M 2009 Overview of physical interaction models for photon and
20 electron transport used in Monte Carlo codes *Metrologia* **46** S112–38
- 21 Schuemann J, McNamara A L, Ramos-Méndez J, Perl J, Held K D, Paganetti H, Incerti S and
22 Faddegon B 2019a TOPAS-nBio: An Extension to the TOPAS Simulation Toolkit for
23 Cellular and Sub-cellular Radiobiology *Radiation Research* **191** 125
- 24 Schuemann J, McNamara A L, Warmenhoven J W, Henthorn N T, Kirkby K J, Merchant M J,
25 Ingram S, Paganetti H, Held K D, Ramos-Mendez J, Faddegon B, Perl J, Goodhead D T,
26 Plante I, Rabus H, Nettelbeck H, Friedland W, Kundrát P, Ottolenghi A, Baiocco G,
27 Barbieri S, Dingfelder M, Incerti S, Villagrasa C, Bueno M, Bernal M A, Guatelli S,
28 Sakata D, Brown J M C, Francis Z, Kyriakou I, Lampe N, Ballarini F, Carante M P,
29 Davidková M, Štěpán V, Jia X, Cucinotta F A, Schulte R, Stewart R D, Carlson D J,
30 Galer S, Kuncic Z, Lacombe S, Milligan J, Cho S H, Sawakuchi G, Inaniwa T, Sato T, Li
31 W, Solov'yov A V, Surdutovich E, Durante M, Prise K M and McMahon S J 2019b A
32 New Standard DNA Damage (SDD) Data Format *Radiation Research* **191** 76
- 33 Semenenko V A and Stewart R D 2004 A Fast Monte Carlo Algorithm to Simulate the Spectrum
34 of DNA Damages Formed by Ionizing Radiation *Radiation Research* **161** 451–7
- 35 Semenenko V A and Stewart R D 2006 Fast Monte Carlo simulation of DNA damage formed by
36 electrons and light ions *Physics in Medicine and Biology* **51** 1693–706
- 37 Stewart R D, Yu V K, Georgakilas A G, Koumenis C, Park J H and Carlson D J 2011 Effects of
38 Radiation Quality and Oxygen on Clustered DNA Lesions and Cell Death *Radiation*
39 *Research* **176** 587–602
- 40 Stewart R D, Streitmatter S W, Argento D C, Kirkby C, Goorley J T, Moffitt G, Jevremovic T,
41 Sandison G A 2015 Rapid MCNP simulation of DNA double strand break (DSB) relative
42 biological effectiveness (RBE) for photons, neutrons, and light ions. *Physics in Medicine*
43 *and Biology* **60**, 8249-74
- 44 Stewart R D, Carlson D J, Butkus M P, Hawkins R, Friedrich T, Scholz M 2018 A comparison
45 of mechanism-inspired models for particle relative biological effectiveness (RBE).
46 *Medical Physics* **45** e925-e952

1 Stewart R D 2018 Induction of DNA Damage by Light Ions Relative to ⁶⁰Co gamma-rays
2 *International Journal of Particle Therapy* **5** 25-39

3 Streitmatter S W, Stewart R D, Jenkins P A, Jevremovic T 2017 DNA double strand break
4 (DSB) induction and cell survival in iodine-enhanced computed tomography (CT)
5 *Physics in Medicine and Biology* **62** 6164-6184

6 Taleei R and Nikjoo H 2012 Repair of the double-strand breaks induced by low energy electrons:
7 A modelling approach *International Journal of Radiation Biology* **88** 948-53

8 Taschereau R, Roy R and Pouliot J 2003 A comparison of methods to calculate biological
9 effectiveness (RBE) from Monte Carlo simulations *Medical Dosimetry* **28** 21-6

10 Thomson R M and Kawrakow I 2018 Quantum versus classical Monte Carlo simulation of low-
11 energy electron transport in condensed amorphous media *Physica Medica* **54** 179-88

12 Thomson R M and Kawrakow I 2011 On the Monte Carlo simulation of electron transport in the
13 sub-1 keV energy range *Medical Physics* **38** 4531-4

14 Villagrasa C, Bordage M-C, Bueno M, Bug M, Chiriotti S, Gargioni E, Heide B, Nettelbeck H,
15 Parisi A and Rabus H 2019 Assessing the contribution of cross sections to the uncertainty
16 of Monte Carlo calculations in micro- and nanodosimetry *Radiation Protection*
17 *Dosimetry* **183** 11-6

18 Wang L L W and Rogers D W O 2010 Replacement correction factors for plane-parallel ion
19 chambers in electron beams: Replacement correction factors plane-parallel chambers in
20 electron beams *Medical Physics* **37** 461-5

21 Ward J F 1988 DNA damage produced by ionizing radiation in mammalian cells: identities,
22 mechanisms of formation, and reparability *Prog. Nucleic Acid Res. Mol. Biol.* **35** 95-125

23 Wu C S, Kliauga P and Amols H I 1996 Microdosimetric evaluation of relative biological
24 effectiveness for ¹⁰³Pd, ¹²⁵I, ²⁴¹Am, and ¹⁹²Ir brachytherapy sources *International*
25 *Journal of Radiation Oncology*Biology*Physics* **36** 689-97

26 Wu C S and Zaider M 1998 A calculation of the relative biological effectiveness of ¹²⁵I and
27 ¹⁰³Pd brachytherapy sources using the concept of proximity function *Medical Physics* **25**
28 2186-9

29 Zaider M, Bardash M and Fung A 1994 Molecular Damage Induced Directly and Indirectly by
30 Ionizing Radiation in DNA *International Journal of Radiation Biology* **66** 459-65
31
32

1 **FIGURE CAPTION**

2

3 **Figure 1:** Microdosimetric quantities y_F (panel a) and y_D (panel b) as a function of the kinetic
4 energy of the primary electron for target spheres of different diameter. The calculations are based
5 on the Opt2 constructor (default models) of Geant4-DNA.

6

7 **Figure 2:** The effect of target diameter on the calculation of y_F (panel a) and y_D (panel b) with
8 the target of $d=2.0$ nm used as the baseline for comparison. The calculations are based on the
9 Opt2 constructor (default models) of Geant4-DNA.

10

11 **Figure 3:** The effect of physics models on the calculation of y_F (panel a) and y_D (panel b) for
12 different target diameters with the Opt2 constructor (default models) used as the baseline for
13 comparison.

14

15 **Figure 4:** Direct DSB yield ($Gy^{-1}cell^{-1}$) as a function of the electron energy for different target
16 diameters obtained with the Opt2 constructor (default models) of Geant4-DNA, for a total DNA
17 length of 6.4 Gbp.

18

19 **Figure 5:** The effect of target diameter on the calculation of the direct DSB yield ($Gy^{-1}cell^{-1}$)
20 with the target of $d=2.0$ nm used as the baseline for comparison. The calculations are based on
21 the Opt2 constructor (default models) of Geant4-DNA.

22

1 **Figure 6:** The effect of physics models on the calculation of the direct DSB yield ($Gy^{-1}cell^{-1}$)
2 for different target diameters with the Opt2 constructor (default models) used as the baseline for
3 comparison.

4
5 **Figure 7:** Frequency distributions of events (tracks) with energy deposition in the target (here
6 3.4 nm diameter sphere) above E for (a) 300 eV incident electrons, (b) 1 keV incident electrons,
7 and (c) 10 keV incident electrons. The calculations are based on the Opt2 (default models) and
8 Opt4 (Ioannina models) constructors of Geant4-DNA. The yellow-shaded area represents the
9 difference between the frequency of Opt4 minus the frequency of Opt2.

10
11 **Figure 8:** Comparison of direct DSB yield ($Gy^{-1}cell^{-1}$) as a function of electron energy. Red
12 circles with full-line: present results with Opt2 constructor (default models); Red circles with
13 broken-line: present results with Opt4 constructor (Ioannina models); Yellow diamonds with
14 full-line: Lampe *et al* (2018a) data with Opt2 constructor (default models); Yellow diamonds
15 with broken-line: Lampe *et al* (2018a) data with Opt4 constructor (Ioannina models); Yellow
16 diamonds with dash-dot-line: Lampe *et al* (2018a) data with Opt6 constructor (CPA100 models);
17 Blue squares: Nikjoo *et al* (1997, 1999, 2001) data; Green circles: Nikitaki *et al* (2016) data;
18 Triangles: Friedland *et al* (1998) data; Squares: Bernal *et al* (2015) data; Purple triangles: Pater
19 *et al* (2014) data; Crosses: Liu *et al* (2017) data; Circles: Frankenberg *et al* (1986) data; Full-line:
20 MCDS calculations with $O_2=21\%$ and $DMSO=0\%$.

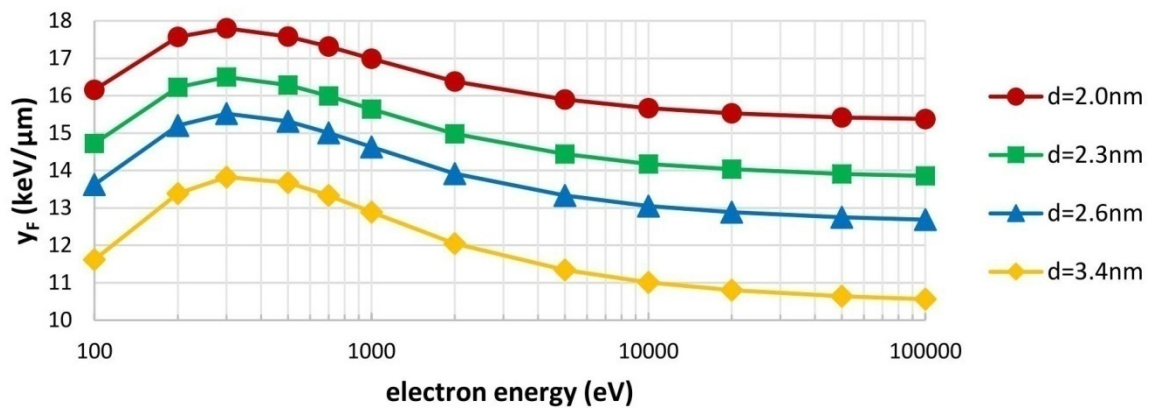
21

1 **Figure 9:** The overestimation of y_F (panel a) and y_D (panel b) for different tracking cutoff
2 energies with 10 eV tracking cut used as the baseline for comparison. The calculations are based
3 on the Opt2 constructor (default models) of Geant4-DNA using a spherical target of $d=2$ nm.

4
5 **Figure 10:** The overestimation of the direct DSB yield ($Gy^{-1}cell^{-1}$) for different tracking
6 cutoff energies with the 10 eV tracking cut used as the baseline for comparison. The calculations
7 are based on the Opt2 constructor (default models) of Geant4-DNA using a spherical target of
8 $d=2$ nm.

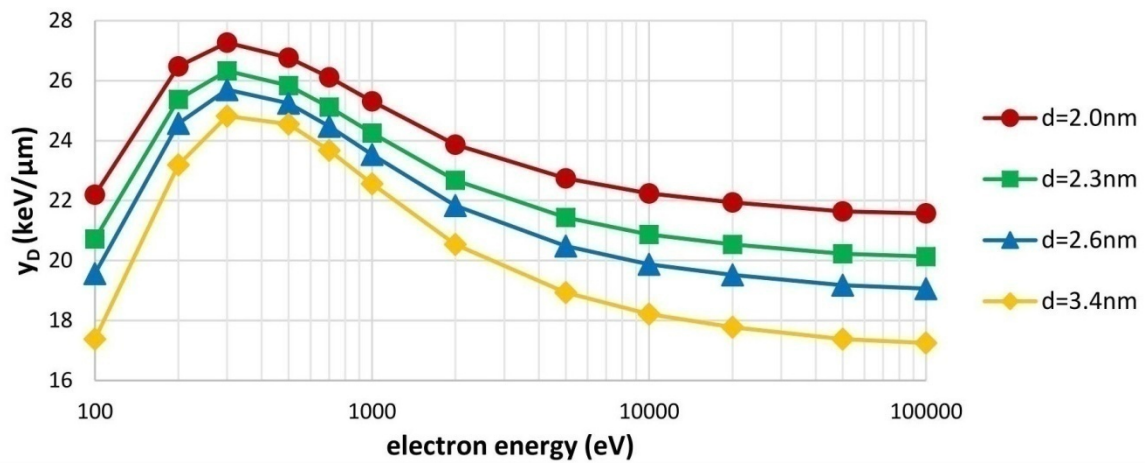
9
10 **Figure 11:** Clustered DSB damage (direct contribution only) induced as a function of electron
11 energy. With the symbol A we denote our calculations with $E_{SSB}=10.79$ eV and with symbol B
12 our calculations with $E_{SSB}=17.5$ eV. Red circles with full-line: present results with Opt2
13 constructor (default models) and $E_{SSB}=17.5$ eV; Red circles with broken-line: present results with
14 Opt4 constructor (Ioannina models) and $E_{SSB}=17.5$ eV; Green triangles with full-line: present
15 results with Opt2 constructor (default models) and $E_{SSB}=10.79$ eV; Green triangles with broken-
16 line: present results with Opt4 constructor (Ioannina models) and $E_{SSB}=10.79$ eV; Blue squares:
17 Nikjoo *et al* (1997) data; Yellow diamonds with full-line: Lampe *et al* (2018a) data with Opt2
18 constructor (default models); Yellow diamonds with broken-line: Lampe *et al* (2018a) data with
19 Opt4 constructor (Ioannina models); Yellow diamonds with dash-dot-line: Lampe *et al* (2018a)
20 data with Opt6 constructor (CPA100 models); Full-line: MCDS calculations with $O_2=21\%$ and
21 DMSO=0%.

22



1

2 **FIGURE 1a**

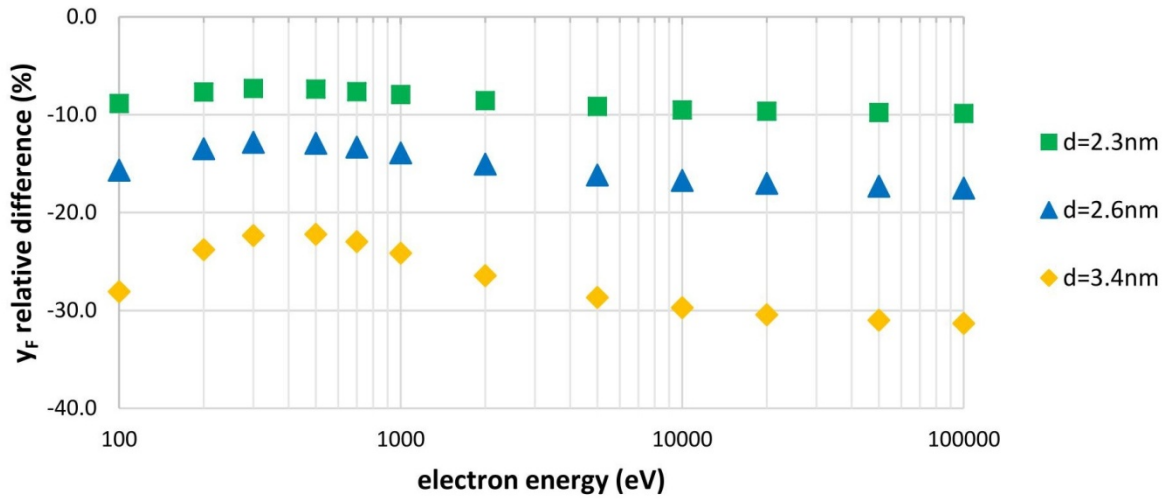


3

4 **FIGURE 1b**

5

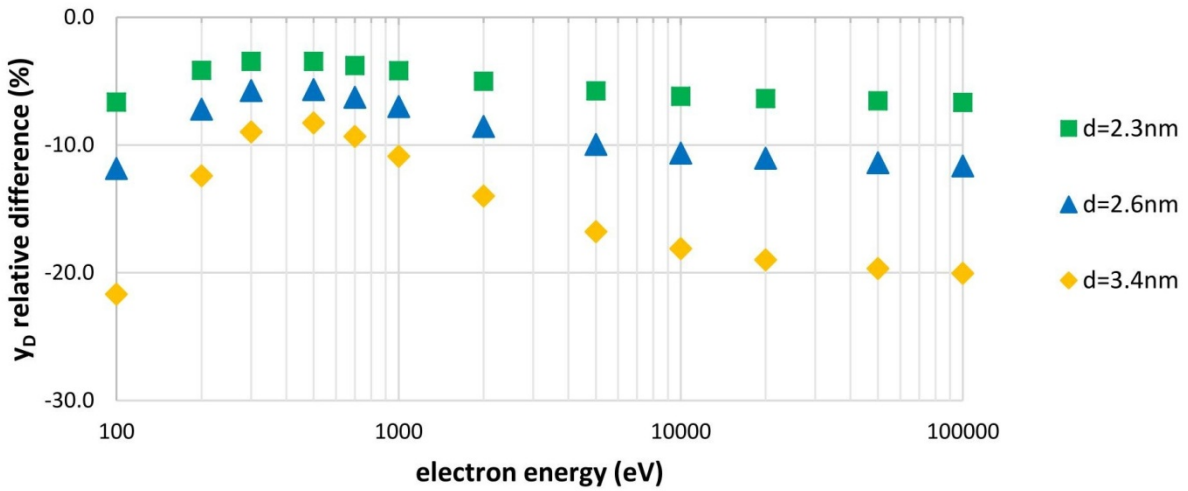
d=2.0nm as baseline



1

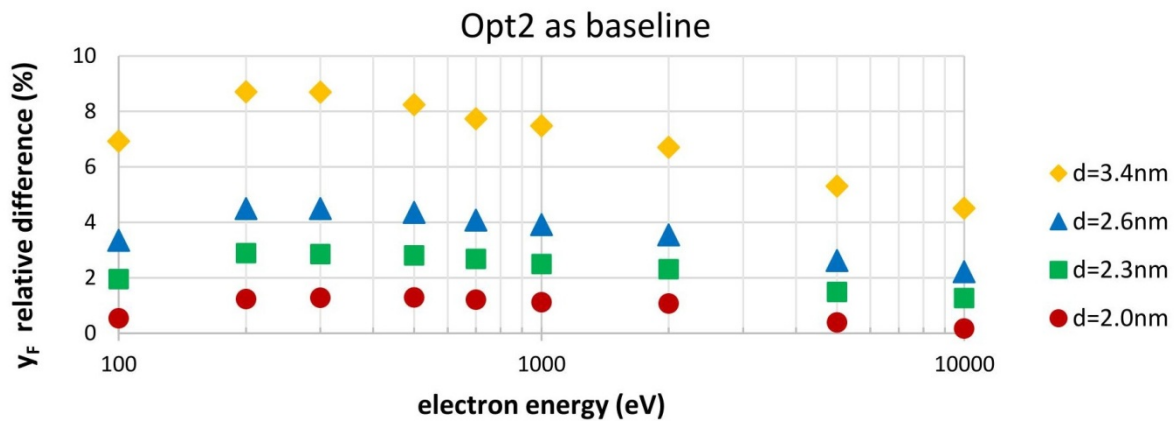
2 **FIGURE 2a**

d=2.0nm as baseline



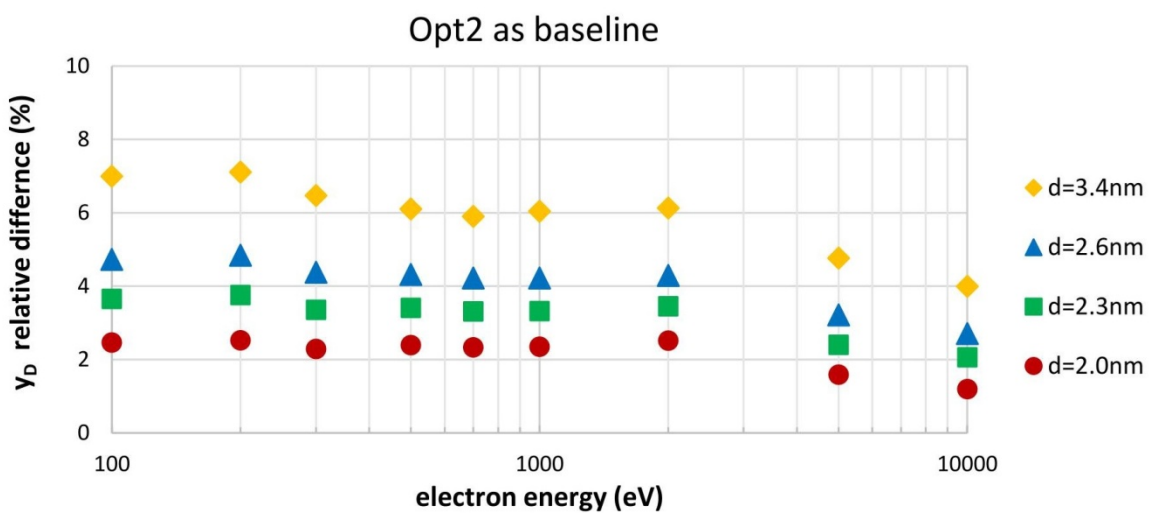
3

4 **FIGURE 2b**



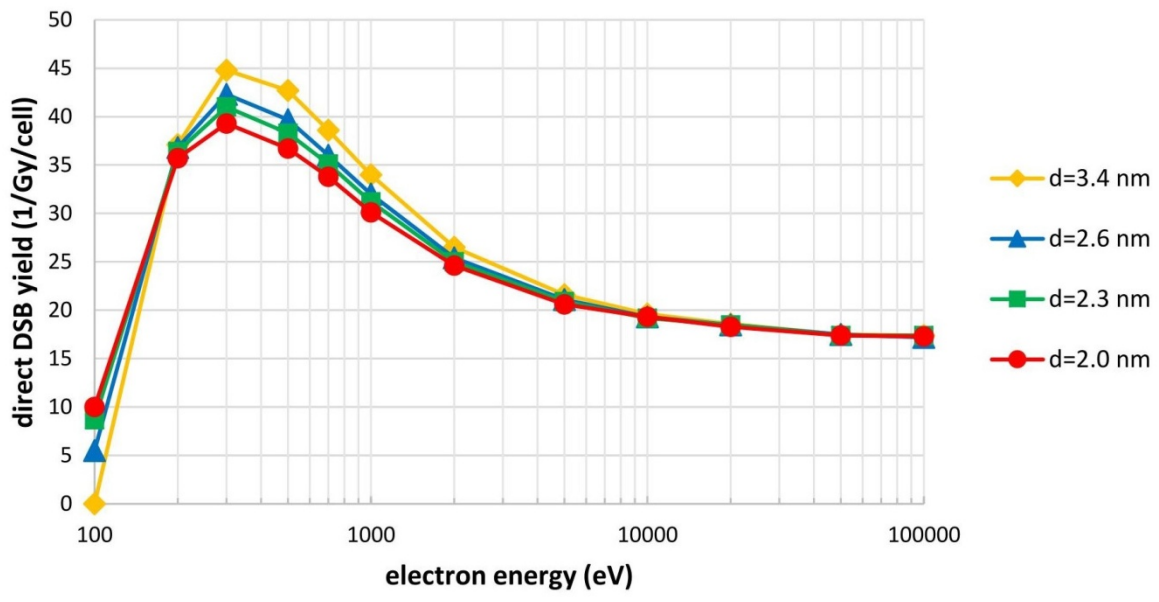
1

2 **FIGURE 3a**



3

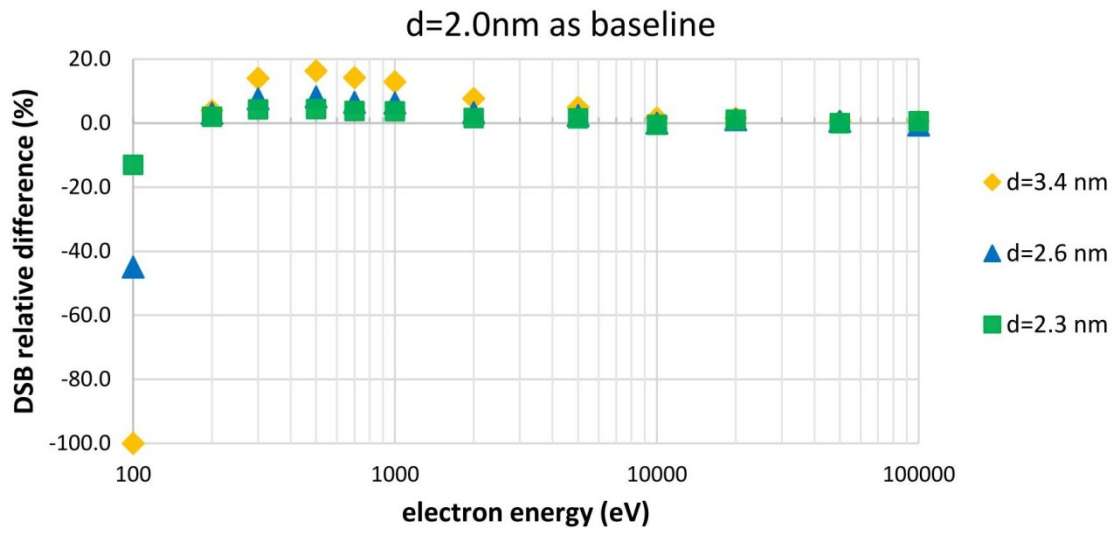
4 **FIGURE 3b**



1

2 **FIGURE 4**

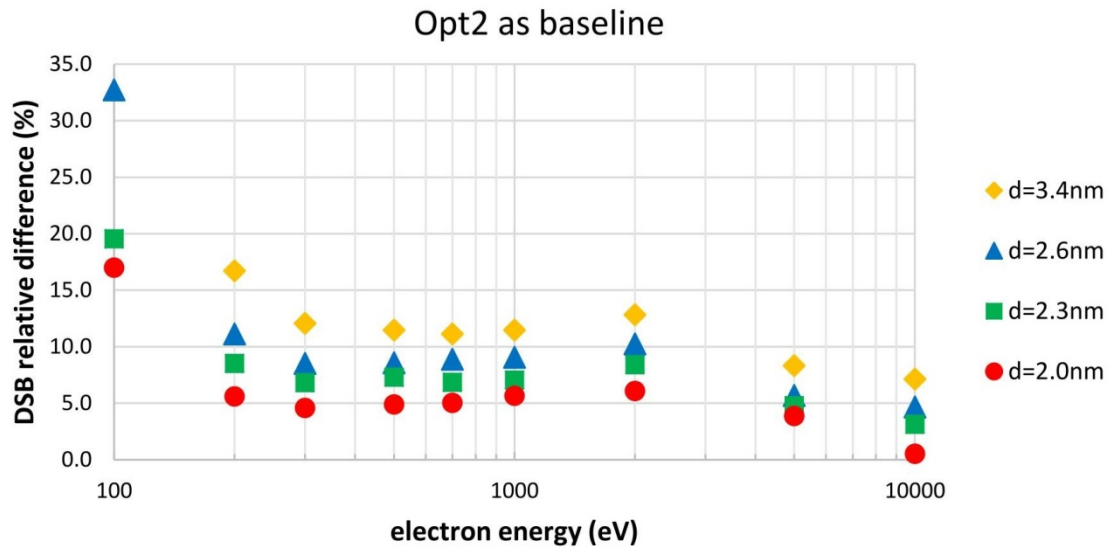
3



1

2 **FIGURE 5**

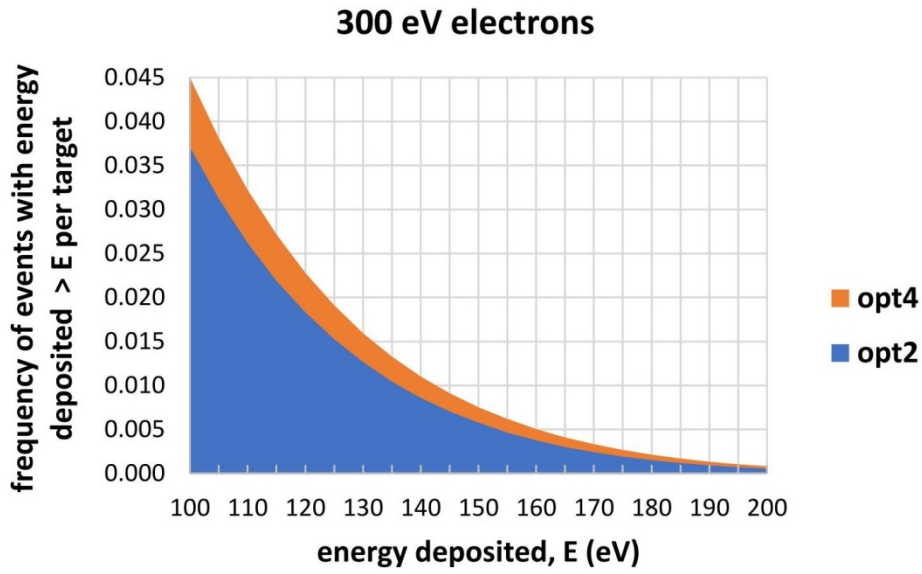
3



1

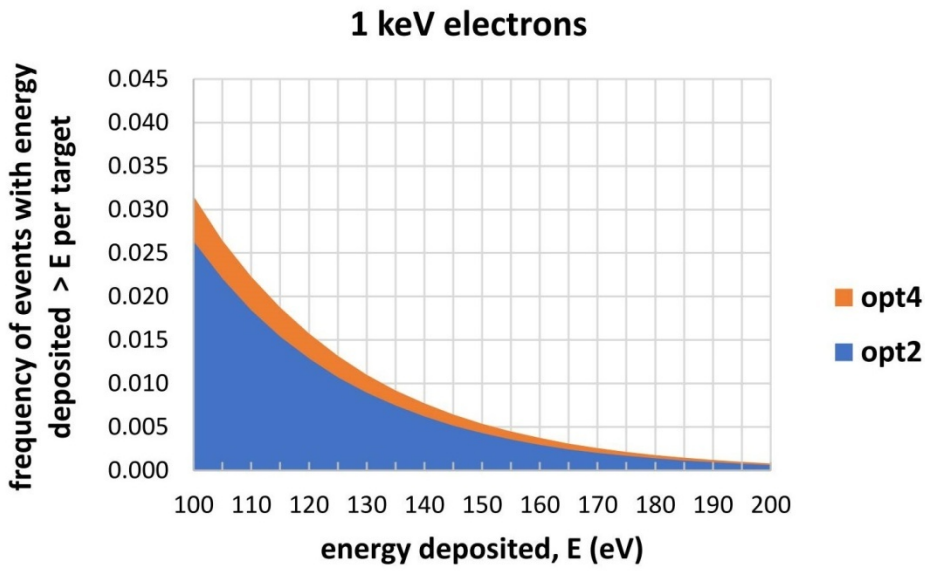
2 **FIGURE 6**

3



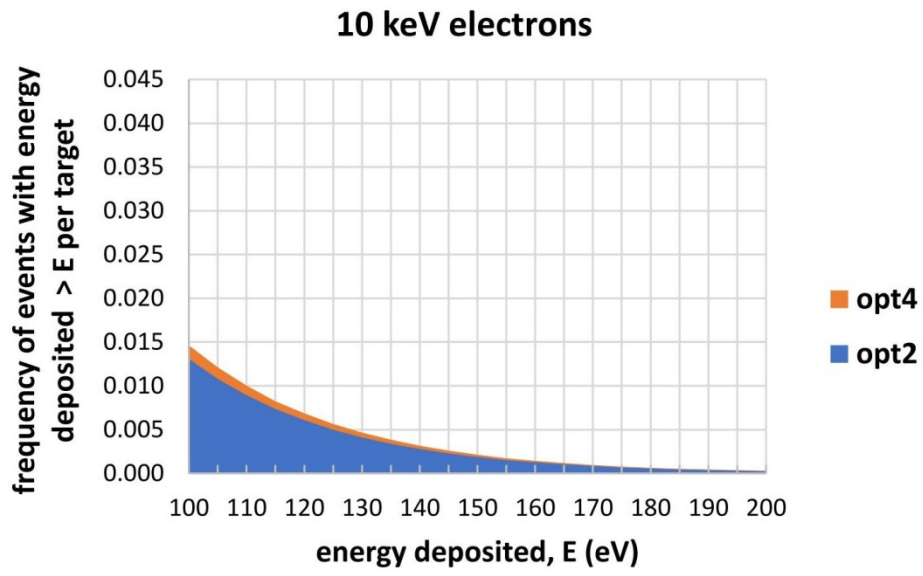
1

2 **FIGURE 7a**



3

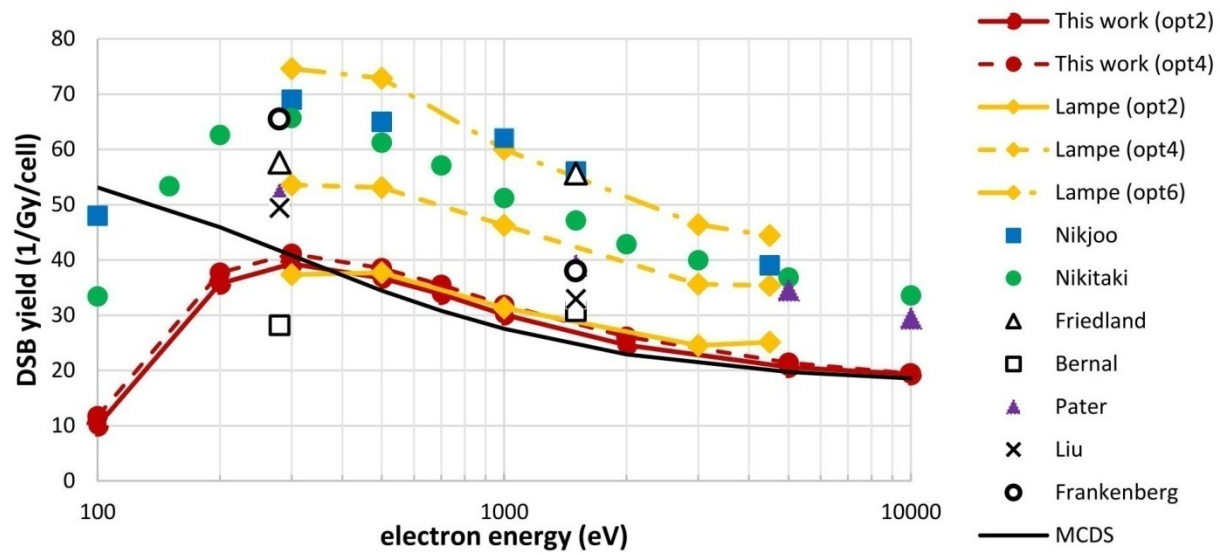
4 **FIGURE 7b**



1

2 **FIGURE 7c**

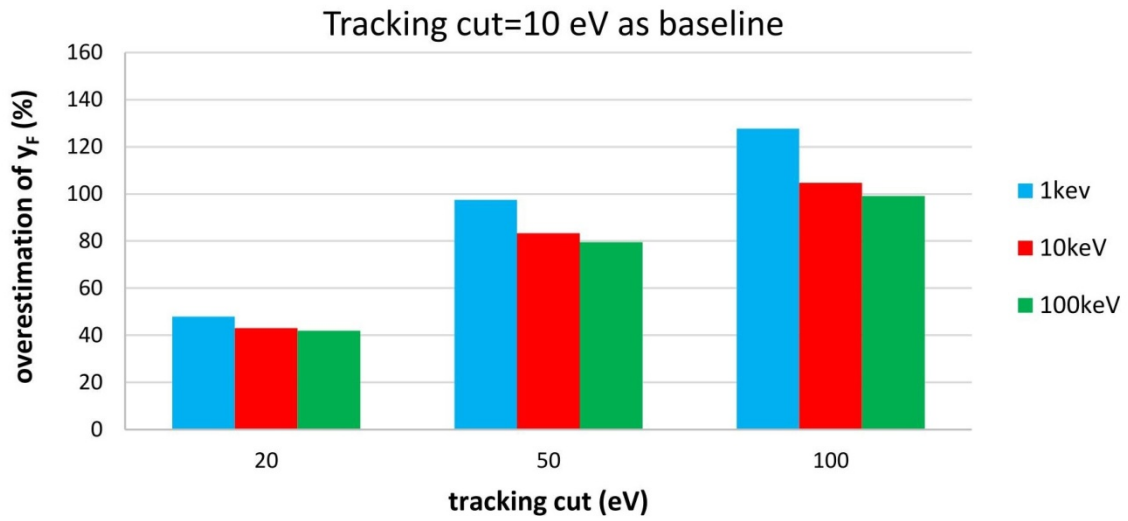
3



1

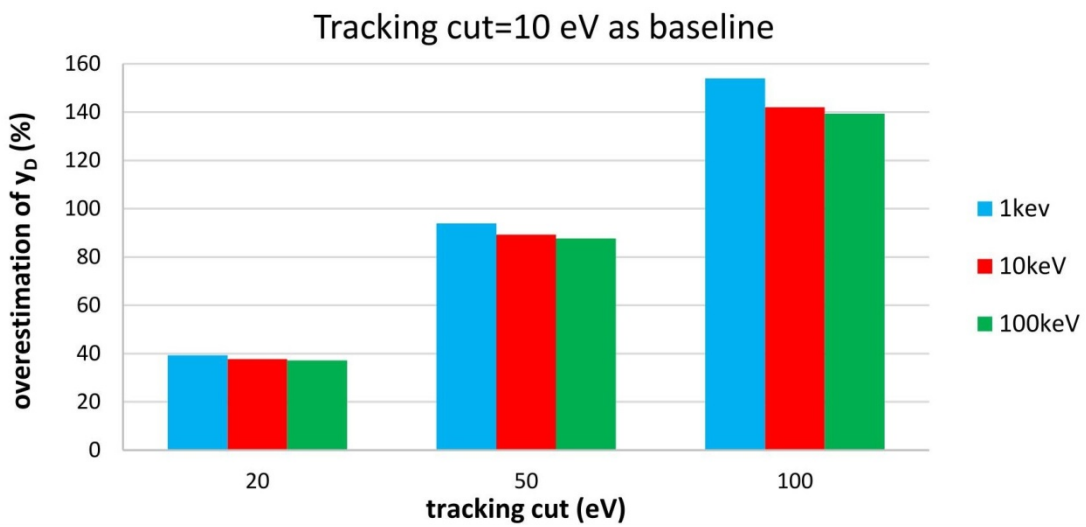
2 **FIGURE 8**

3



1

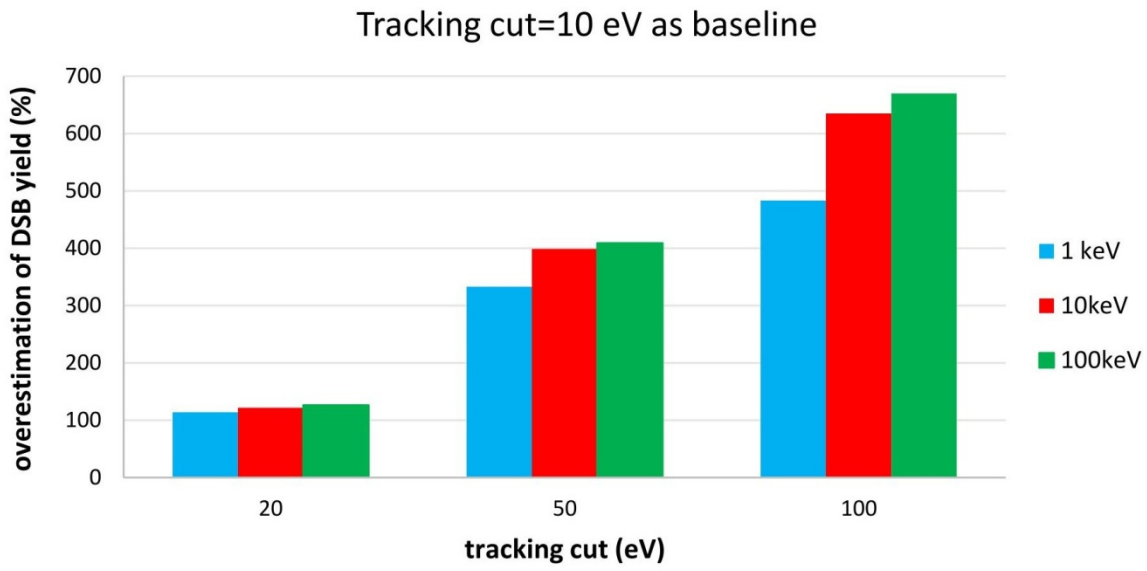
2 **FIGURE 9a**



3

4 **FIGURE 9b**

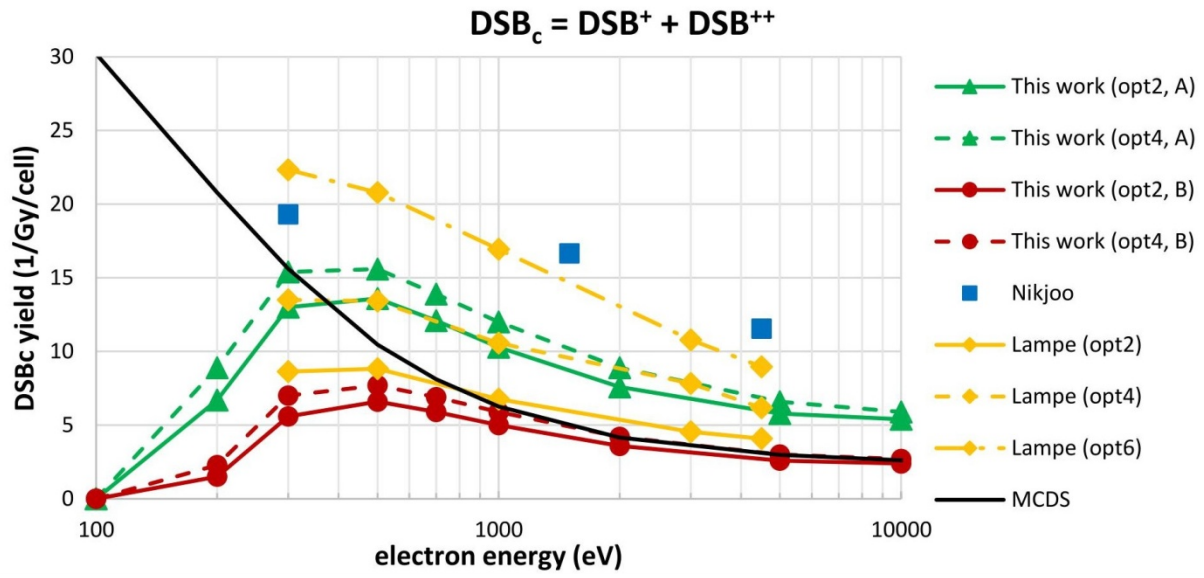
5



1

2 **FIGURE 10**

3



1

2 **FIGURE 11**

3

4

5

6